Hydrogel effects rapid biofilm debridement with *ex-situ* contact-kill to eliminate multi-drug resistant bacteria *in vivo*

Chun Kiat Yeo[1,2], Yogesh Shankar Vikhe[2,3], Peng Li[2], Zanru Guo[2], Peter Greenberg[4], Hongwei Duan[2,3], Nguan Soon Tan[5]*, Mary B. Chan-Park*[2,3]

[1]NTU Institute for Health Technologies, Interdisciplinary Graduate School, Nanyang Technological University, Singapore 637553

[2]School of Chemical and Biomedical Engineering, Nanyang Technological University, 62 Nanyang Drive, Singapore 637459

[3]Centre for Antimicrobial Bioengineering, Nanyang Technological University, Singapore 637459

[4]Department of Microbiology, University of Washington School of Medicine, Seattle, Washington, 98195-7735, USA

[5]School of Biological Sciences, Nanyang Technological University, Singapore 637551

*E-mail: mbechan@ntu.edu.sg; NSTan@ntu.edu.sg

Keywords: antibacterial, hydrogel, infection, wound, biofilm-debridement

ABSTRACT

Multi-drug resistance and the refractory character of bacterial biofilms are among the most difficult challenges in infection treatment. Current antimicrobial strategies typically are much more effective for prevention of biofilm formation than for eradication of established biofilms; these strategies also leave dead bacteria and endotoxin in the infection site, which impairs healing. We report a novel hydrogel that eradicates biofilm bacteria by non-leaching-based **d**ebridement followed by ***e**x-**s**itu* **c**ontact-**k**illing (DESCK) away from the infection site. The debridement effect is likely due to the high water swellability and microporosity of the crosslinked network which is made from polyethylene glycol dimethacrylate tethered with a dangling polyethylenimine (PEI) star copolymer. The large pore size of the hydrogel makes the cationic pore walls highly accessible to bacteria. The hydrogel also degrades in the presence of infection cells, releasing star cationic PEI into the infection site to contact-kill bacteria remaining there. DESCK hydrogel effectively kills (>99.9% reduction) biofilms of methicillin-resistant *Staphylococcus aureus* (MRSA) and carbapenem-resistant *Pseudomonas aeruginosa* (CR-PA) and *Acinetobacter baumannii* (CR-AB) in a murine excisional wound infection model. Silver-based wound dressings (controls) showed almost no killing of CR-PA and MRSA biofilms. This DESCK hydrogel greatly reduces the bioburden and inflammation, and promotes wound healing. It has great potential for diverse infection treatment applications.

INTRODUCTION

Bacterial infections begin with colonization by planktonic pathogens but by the time of diagnosis, they usually have progressed beyond colonization to formation of biofilm. Biofilm bacteria are typically difficult to treat with current antibiotics since these are designed to treat metabolically active planktonic bacteria.[1-6] Also, biofilm bacteria are protected by a matrix of extracellular polymeric substances (EPS) which retard the diffusion of antimicrobial agents.[7] The antibiotic concentration required to kill bacteria in biofilm can be as much as 1000x that required to kill planktonic bacteria.[6, 8-9] This problem is compounded by the inevitable, and now widespread, emergence of resistance to conventional antibiotics. Infections with multi-drug resistant (MDR) bacteria in biofilm form are difficult to treat, particularly in hospitalized patients who may be immunocompromised.

Various strategies other than antibiotics, such as silver and metal-derived formulations, and contact-active cationic polymers, have been investigated to address the challenge of eradication of biofilms of MDR bacteria. These strategies typically prevent biofilm formation but do not treat established infection. Silver-derived formulations have been extensively investigated in wound dressings, catheters, coatings, *etc.*[10-14] However, various studies have indicated that silver eradicates planktonic but not biofilm bacteria.[15-17] Non-silver based treatments have been studied but is rather prophylactic.[18] An alternative bactericidal mechanism, such as contact-kill by cationic hydrogel, is desirable from the standpoint of avoiding harm to tissue from released toxic materials. However, hitherto, contact-active hydrogels suffer from the drawback that bacteria within the infected tissue or protected in the biofilm may not come into contact with the cationic polymer network. Various antibacterial

contact-active hydrogel coatings have been reported[19-20] but these are typically for prophylactic treatment of bacteria and do not eradicate biofilm bacteria. Debridement (*i.e.* removal of bacteria and endotoxin from the infection site) by enzymes has been reported[21-22] but not by non-leaching mechanisms such as diffusion or advection in fluid flow as reported here. Debridement can reduce inflammation and is critically important for the healing of chronic wounds.[23-24] Debridement resulting in bacterial translocation away from the infection site followed by *ex-situ* killing is a novel concept for anti-biofilm contact-active hydrogel.

We describe herein the first demonstration of a hydrogel that eradicates biofilm bacteria by non-leaching-based **d**ebridement followed by ***e*x-*s*itu** **c**ontact-**k**illing (DESCK) away from the infection site. The hydrogel network is made from a star polyethylenimine(PEI)-derived methacrylated copolymer (Scheme 1a(i)) and a poly(ethylene) glycol dimethacrylate (PEGDMA) crosslinker (Scheme 1a(ii)). The PEI copolymer (molecular weight 25 kDa) has low grafting density of methacrylate group, about 1 per PEI molecule and would dangle from the hydrophilic crosslinked PEGDMA network. The hydrogels are highly swellable and have pores of 10 – 20 μm in diameter which are larger than bacteria to minimize clogging. The DESCK hydrogel causes debridement -- it absorbs biofilm bacteria from the wound into itself to a depth of 10 – 20 μm -- probably because of diffusion and slow fluid flow into the hydrogel. Bacteria absorbed into the hydrogel are *ex-situ* contact-killed by the cationic pore walls (Scheme 1b - mode 1). Further, the infection also triggers the release of the bactericidal cationic PEI polymer from the hydrogel network to kill bacteria at the infection site which is distant from the hydrogel (Scheme 1b - mode 2). This new hydrogel effectively treats and prevents bacterial biofilm infections in a mouse wound model of carbapenem-resistant *Pseudomonas*

aeruginosa and *Acinetobacter baumannii* – which is declared critical by the World Health Organization (WHO),[25] as well as of methicillin-resistant *Staphylococcus aureus* (MRSA). In both its prophylactic and treatment modes, the hydrogel reduces bacterial load by several orders of magnitude, which bettered silver-based wound dressings (controls).

RESULTS

Four series of hydrogel formulations were prepared (Table 1). Hydrogel Series 1 is composed of (10 wt%) polyethylenimine-*graft*-polyethylene glycol methacrylate (PEI-PEGMA) (Scheme 1a(i)) mixed with (10 wt%) polyethylene glycol dimethacrylate (PEGDMA). A PEI with molecular weight (M_w) of 25 kDa was used; five PEI(25K)-PEGMA (1:x) copolymers were made with varying molar ratios of PEGMA (x = 1, 2, 3, 4 and 6) to PEI for formulations 1a – 1e respectively (Supporting Scheme S1.1): (1a) PEI(25K)-PEGMA (1:1), (1b) PEI(25K)-PEGMA (1:2), (1c) PEI(25K)-PEGMA (1:3), (1d) PEI(25K)-PEGMA (1:4) and (1e) PEI(25K)-PEGMA (1:6). The ^{1}H NMR characterization of the chemical structures of the polymers is presented in Supporting Figure S1.2. The actual grafting ratios of PEGMA to PEI (mole/mole) were measured via titration of the double bond content and found to be 1.25, 1.83, 3.02, 4.24 and 5.96 for polymers 1a – 1e respectively (Table 1).

For Series 2 and 3, we used a lower, as well as a higher, molecular weight PEI (800 and 750K Daltons) to obtain (2) PEI(800)-PEGMA (1:1) and (3) PEI(750K)-PEGMA (1:6) respectively; the respective titrated grafting ratios (mole/mole) were measured to be 0.9 and 6.50 (Table 1). To study the effect of hydrophobicity, we also added a second graft of decane to make the 4th series: PEI(25K)-decane-PEGMA (1:10:2) (Scheme 1a(iii)). (^{1}H NMR

spectrum of this graft copolymer in Supporting Figure S1.3 confirms the chemical structure of this copolymer.) The titrated PEGMA grafting per PEI ratio (mole/mole) is 2.08 (Table 1).

The *in vitro* contact killing efficacies of the hydrogels were measured against various multi-drug resistant Gram-negative and Gram-positive bacteria (Table 1). The bacterial log reduction results show that Series 1a (with lowest PEGMA grafting ratio), Series 3 and Series 4 totally eradicated the various bacteria loaded onto the hydrogel discs; the bacteria eradicated include ESKAP (*i.e. Escherichia coli* (*E. coli*), *Staphylococcus aureus* (*S. aureus*), *Klebsiella pneumoniae* (*K. pneumoniae*), *Acinetobacter baumannii* (*A. baumannii*, AB) and *Pseudomonas aeruginosa* (*P. aeruginosa*, PA), including methicillin-resistant *S. aureus* (MRSA USA300) and carbapenem-resistant Gram-negative AB and PA strains (CR-AB and CR-PA), which are pathogens of great concern worldwide.[21, 25] The other hydrogels (1b - 1e and Series 2) do not completely eradicate the bacteria. An agar diffusion test performed with *P. aeruginosa* PA01 using Series 1a and Series 4 (together with a control - PEGDMA) hydrogels proved that bacteria were killed by contact with the gels instead of leaching of residual uncured cationic polymers as no zones of inhibition (Supporting Figure S2.1) were observed.

The two hydrogels (both with 25 kDa PEI) that showed the highest *in vitro* bacterial killing were chosen for further characterizations and comparisons; Series 1a and Series 4 are hereinafter respectively denoted as PEI(1a) and PDP. The *in vitro* viabilities of human dermal fibroblasts (HDF) when tested via Transwell and contact MTT assays were close to 100% and 90% respectively for both formulations (Figure 1a), indicating low acute toxicity of these two hydrogels. This good biocompatibility is due to negligible leaching (Supporting Figure S2.2) and high hydration of the charged hydrogel.

These hydrogels are transparent (Figure 1b) and swell significantly and rapidly in water: PEI(1a) and PDP hydrogels swelled by 11.7x and 11.3x (final mass/initial mass) respectively within 15 min of immersion into water (Figure 1c). Also, the water-equilibrated PEI(1a) and PDP hydrogels have relatively good compressive strengths at 50% strain of 119±6.9 kPa and 12.3±1.1 kPa respectively and also good ultimate compression strains of more than 50% (Supporting Figure S2.3). The contact angles of water on PEI(1a) hydrogel after 0 min and 2 min of water droplet deposition were measured to be 21.8°±2.1° and 11.4°±1.2° respectively while those of PDP hydrogel were higher (50.6°±3.1° and 30.6°±2.4° respectively, Supporting Figure S2.4), corroborating that the decane graft increases the hydrophobicity of the PDP hydrogel.

Using the LIVE/DEAD assay, we show that all bacteria inoculated on the PEI(1a) hydrogels were dead and stained red (Figures 1d(i, ii)), indicating permeabilized membranes. On the control hydrogel (PEGDMA), all bacteria were stained green, indicating live bacteria (Figures 1e(i, ii)). Freeze-dried hydrogels were examined by field emission-scanning electron microscopy (FE-SEM). The PEI(1a) hydrogel is microporous with pores larger than 10 μm (Figure 1f(i)). FE-SEM images of PEI(1a) hydrogels inoculated with MRSA USA300 and PA01 (Figures 1f(ii, iii)) show that the bacteria are attached to the pore walls and experience severe membrane perturbation. Bacterial debris can be seen sticking to the hydrogel wall (Figures 1f(ii, iii), arrows), likely because of cell lysis and release of cellular contents. The control hydrogel (PEGDMA) is also microporous (Figure 1g(i)) and does not appear to affect the morphology or membrane integrity of the bacteria loaded (Figures 1g(ii, iii)). The bactericidal effect of PDP hydrogel is similar to that of PEI(1a) hydrogel (Supporting Figures

S2.5 and S2.6). Hence, the LIVE/DEAD assay and FE-SEM results show that PEI(1a) and PDP hydrogels are contact-active and bactericidal.

The *in vivo* bactericidal activities of PEI(1a) and PDP hydrogels against Gram-negative and Gram-positive bacteria were tested with a murine excisional wound infection model using MRSA USA300, CR-AB, CR-PA and PA01 and were compared with commercial silver-based antimicrobial wound dressings (specifically Allevyn Ag and Algisite Ag from Smith & Nephew; both employ silver as antimicrobial agent). After wound creation and infection, the wounds were treated by application of a wound dressing for one day starting either almost immediately for the prophylactic treatment model or 24 h post-infection for the anti-biofilm treatment model.

In the anti-biofilm treatment model, the PEI(1a) hydrogel showed greater than 3 log reduction (>99.9%) for all four tested bacteria (MRSA, CR-AB, CR-PA and PA01) (Figures 2a-e). This is superior to the generally ineffective treatment (<1.0 log reduction) with Allevyn Ag (Figures 2a-e); Algisite Ag was also ineffective (<1.0 log reduction) against PA01, CR-PA and MRSA (Figures 2a, c-e) though it moderately suppressed CR-AB (with 2.1 log reduction, Figures 2b, e). Hence, the PEI(1a) hydrogel is broad spectrum and significantly kills (>3 log reduction) the MDR biofilm bacteria tested, which the Ag-based wound dressings did not. PDP hydrogel also generally outperformed the Ag-based wound dressings with more than 3 log reduction for MRSA and more than 2 log reduction for all the Gram-negative strains (Figure 2). We also studied the dynamics of biofilm bacteria (MRSA USA300) reduction at the wound site over a period of seven-day treatment with the different dressings. Most of the reduction in wound bacteria occurred during the first day of treatment, after which bacterial counts

remained almost constant (Figure 2f).

We also investigated the bactericidal effect with an *in vivo* prophylactic model, *i.e.* the wound dressing was applied almost immediately (10 min or 0^+ h) after bacteria inoculation. In the prophylactic model, the PEI(1a) hydrogel achieved >4.0 log reduction (>99.99%) for all 4 tested bacteria (Figure 3a and Supporting Figure S3.1). These bactericidal effects were also better than those of the Ag-based Allevyn Ag and Algisite Ag dressings (by about 2 log and 1 log respectively). Hence, it appears that the Ag-based wound dressings work fairly well for prophylactic treatment involving planktonic bacteria (Figure 3a) but do not generally kill biofilm bacteria (Figure 2e), corroborating published results.[17]

We also studied the healing of MRSA USA300 infected wounds over a 2-week period using the prophylactic treatment with PEI(1a) hydrogel (Figure 3b). At days 7, 9, 12 and 14 post-infection, the sizes (normalized to the initial wound size) of the PEI(1a) hydrogel treated wounds were much smaller than the control wounds. Moreover, over the entire duration, the PEI(1a) hydrogel treated wounds were cleaner than the control wounds; much more pus were observed on the control wounds (Figure 3c). Furthermore, secondary wound sites were seen on the control wounds only; these were most likely caused by the spread of infection from the wound site to nearby skin areas (Figure 3c, arrows). Histological analysis of skin tissues beside the wound bed on day 3 showed reduced inflammation for the PEI(1a) hydrogel treated wound as compared with untreated infected wound (Figure 3d). Further analysis by fluorescence-activated cell sorting (FACS) showed that the percentage of $CD11b^+$ cells (*i.e.* leukocytes, which include monocytes, neutrophils, granulocytes and macrophages) increased in untreated infected (by MRSA USA300 and PA01) wounds. However, infected wounds treated with

PEI(1a) hydrogel did not show any excess inflammatory ($CD11b^+$) cells over the levels present in uninfected wounds for both strains of bacteria (Figure 3e), indicating that PEI(1a) hydrogel wound dressing likely reduces the inflammation due to infection by killing and removing bacteria from the wound site. PDP hydrogel, however, did not modulate the number of $CD11b^+$ cells after 3 days.

To investigate the mechanism of the *in vivo* in-wound bacterial count reduction of PEI(1a) hydrogel, we repeated the mouse anti-biofilm wound experiment using fluorescently labelled bacteria, specifically mCherry labelled MRSA USA300 and green fluorescent protein (GFP) labelled PA01. After a 24 h treatment period (the interval during which most of the bacterial count reduction takes place, Figure 2f), the hydrogels were examined by confocal microscopy (Figure 4a). Numerous fluorescent bacteria were observed in the hydrogels up to 25 μm and 15 μm deep for MRSA USA300 and PA01 respectively (as measured from the wound contact surface of the hydrogel) (Figures 4b, c). The bacteria are absorbed into the pore spaces of the hydrogel wound dressing as depicted in Scheme 1b - mode 1.

To examine the influence of the ester linkage degradation on bactericidal effects (Scheme 1b – mode 2), we tested a modified PEI hydrogel in which the ester linkages were replaced with acrylamide (aca) linkages. A new copolymer was synthesized from PEI by linking it to polyethylene glycol acrylamide (PEGACA) instead of PEGMA (Supporting Scheme S1.1c); the new copolymer is PEI(25K)-PEGACA (1:1) (hereinafter called PEI(aca) polymer, Scheme 1a(iv)). Also, the crosslinker used was polyethylene glycol diacrylamide (PEGDACA) instead of PEGDMA in the new hydrogel formulation. Using the 24 h post-infection/24 h treatment model, we observed that PEI(aca) hydrogel achieved 3.1 and 2.2 log reduction of MRSA and

PA01 instead, which is significantly less than the PEI(1a) hydrogel (with 3.9 and 3.1 log reduction respectively) (Figure 4d). Incubation of the PEI(1a) and PEI(aca) with wound fluid shows that PEI(aca) is more stable and releases less of the rhodamine-tagged PEI polymer (Figure 4e) than PEI(1a). No signals were observed for the control fluid (PBS). The less stable PEI(1a) due to degradation of ester linkages by bacterial lipases and leukocyte esterases probably releases the PEI polymer into the wound site to contribute towards the bactericidal effect; on the other hand, the acrylamide bonds in the less bactericidal PEI(aca) hydrogel are degradable only by neutrophil elastase[26] so that less PEI is released from PEI(aca) than from PEI(1a) hydrogel. An *in vitro* experiment conducted by incubating the hydrogel in the presence of bacteria and leukocytes, which are present at the wound sites also confirmed the release of PEI (Supporting Figure S3.2).

DISCUSSION

Rapid debridement of biofilm bacteria is a unique property of this series of hydrophilic and loosely crosslinked hydrogels. The PEI(1a) hydrogel is rapidly highly swellable, and possesses pores that are much larger (10 – 20 μm diameter) than bacterial size so that they do not easily clog. The PEI(1a) hydrogel becomes fully hydrated relatively quickly (in 15 minutes) as compared to the much slower swelling kinetics of many other hydrogels[27-28] which may take hours or even days to reach equilibrium swelling. The rapid swelling of these hydrogels is attributable to the hydrophilicity of both PEG and the star PEI polymer which has high density of protonated amines ($–NH_3^+$), the low crosslink density of the hydrogel network and the high porosity of the hydrogel.

We hypothesize that the combination of large, accessible pores and rapid rehydration promotes absorption of bacteria into the superficial pore spaces of the hydrogel. Non self-motile bacteria such as the species studied here can move by Brownian motion and hydrodynamic drag due to evaporation-driven re-swelling of the hydrogel. The thermal scale height (k_BT/m_bg)[29] is of the order of 10 microns (where k_B is the Boltzmann constant, T is temperature, m_b is buoyant mass (*i.e.* volume of particle x (density of particle – density of body serum)), g is gravitational acceleration))[29]. This scale height (10 μm) is large enough to permit slow vertical migration of bacteria from biofilm into the pore space of a hydrogel pressed into conformal contact with the infected wound. Also, evaporation of wound fluid/exudate from the top surface of the hydrogel probably causes fluid flow into the hydrogel from below, which causes upward hydrodynamic drag on the bacteria, contributing to bacterial translocation from wound to hydrogel. Water evaporates at the rate of 0.722 mg/min.cm^2 at 25 °C (about 500 μm/h of water film thickness) when uncovered[30]. The fluid flow rate necessary to lift bacteria against gravity by itself may be estimated by Stokes' law to be about 200 μm/h (Supporting S4), which is significantly smaller than the flow rate into the hydrogel if it evaporates from its upper surface at a rate comparable to that of uncovered water (Supporting S4). The high degree of hydration of the hydrogel also keeps the wound area moist, which is crucial in the wound healing process.[31-33] Translocation of bacteria from wound to hydrogel is also promoted by dispersal processes intrinsic to mature biofilms, such as surfactant production in *S. aureus* biofilms that normally promotes cell and biofilm fragment detachment and spread of infection from the site of a mature biofilm.[34-35] Importantly, the pore size of our hydrogels is about 10 – 20 μm in diameter which makes the interior pore space highly accessible. Smaller pore sizes

may retard the upward motion of bacteria due to clogging at the hydrogel surface, while larger pores may reduce the accessible internal surface area of hydrogel within easy vertical diffusion distance, retarding bacterial absorption. That PEI(1a) hydrogel has better anti-biofilm killing than alkylated PDP hydrogel (Figure 2) corroborates the hypothesis that hydrophilicity and hence swelling contribute to bacterial absorption out of the wound environment into the hydrogel. The various translocation processes and the destruction of bacteria within the hydrogel significantly reduces bacterial load on the wound site.

The high positive charge of the pore walls due to cationic PEI helps to hold bacteria in place once they diffuse into contact and over time also kills them through membrane perturbation. The Debye length in physiological fluids is of nanometer length scale so that the interaction between anionic bacterial membrane and cationic pore wall is essentially a contact interaction. Our hydrogel absorbs bacteria into its network and then contact-kills the bacteria away from the infection site (*i.e. ex-situ*) to leave the site fairly clean.

The second kill mode ("triggered release") acts against both bacteria trapped in the hydrogel pore spaces and bacteria that remain in the wound. Infection-triggered degradation of the hydrogel network results in release of the bacteria-toxic cationic PEI into the aqueous environment where it can interact with bacteria both in the dressing and in the wound site. While triggered release of cationic agents is a subsidiary kill mode for the PEI(1a) hydrogel, it is not insignificant; the difference in efficacy of PEI(1a) *vs* PEI(aca) *in vivo*, which is attributable to differences in the amount of PEI released, suggests that released PEI contributes about 1 log reduction.

Our PEI(1a) hydrogel is more bactericidal to biofilm bacteria than the two commercial

silver-based wound dressings tested, even to CR-PA and CR-AB which urgently need new antibacterial therapies.[25] The hydrogels effectively cause debridement of the bacteria and kill them *ex-situ* in the hydrogel. Treatment with the PEI(1a) hydrogel left a clean wound, unlike the untreated control wounds that had pus and even secondary infection sites near the infected wound. These hydrogel dressings also improve healing quality by accelerating wound closure and suppressing inflammation. Debridement (Figures 4b, c) followed by *ex-situ* killing is advantageous over conventional *in-situ* destruction of bacteria as removal of bacteria and endotoxin from the wound would be expected to promote healing.

In conclusion, we present a hydrogel which demonstrates a new mechanism for effective biofilm removal *i.e.* non-leaching-based debridement followed by *ex-situ* contact-killing within itself. The high water swelling and microporosity of the hydrogel probably contribute towards its biofilm debridement capability while the dangling high molecular weight (25 kDa) cationic PEI effectively contact-kills bacteria. The hydrogel also kills bacteria in the wound through triggered release of PEI. The PEI(a) hydrogel leaves a cleaner wound throughout the healing process, reduces inflammation and also accelerates wound closure. The DESCK hydrogel effectively eradicates more than 99.9% of multi-drug resistant Gram-positive and Gram-negative biofilm bacteria tested in a mouse excisional wound infection model. The biofilm bacteria reduction is substantially greater than that achieved with silver dressings which can prevent but not treat biofilm PA and MRSA infections. Our PEI(1a) hydrogel also has outstanding *in vivo* prophylactic ability – it eradicates more than 99.99% of planktonic bacteria tested. With minor modifications, this material may also find useful application in coatings on medical devices such as indwelling catheters or implants.

MATERIALS AND METHODS

Chemicals

Branched polyethylenimine (PEI, Sigma-Aldrich, M_w = 800, 25,000 and 750,000) was lyophilized to dryness before use. 1-Bromodecane, sodium hydroxide, potassium carbonate, isopropanol, polyethylene glycol methacrylate (PEGMA, M_n = 360) and 2-hydroxy-4'-(2-hydroxyethoxy)-2-methylpropiophenone (Irgacure 2959) were purchased from Sigma-Aldrich and used as received. Chloroacetyl chloride, absolute ethanol, toluene and methylene chloride were purchased from Merck Pte Ltd (Singapore) and used without further purification. Poly(ethylene glycol) dimethacrylate (PEGDMA, M_n = 1000) was purchased from Polysciences, Inc. Amine-terminated polyethylene glycol acrylamide (PEGACA, M_n = 400) and polyethylene glycol diacrylamide (PEGDACA, M_n = 1000) were purchased from Biochempeg.

Formation of hydrogels

Syntheses of hydrogel polymers are described in Supporting S1. Hydrogels were formed by UV irradiation of the hydrogel precursor solutions. Irgacure 2959, the UV initiator, was first dissolved in ethanol to make a 10% w/v stock solution. Hydrogel solutions containing the PEI polymer (10%), crosslinker (PEGDMA, 10%) and UV initiator (Irgacure 2959, 0.1%) were mixed and dissolved completely in deionized water in a 1.5 mL microtube. Hydrogel solution (50 μL) was transferred to each well of a 96-well plate. The solutions were then irradiated with UV light (365 nm, 18 mW cm^{-2}) for 10 min to crosslink the precursor solutions into hydrogels. The hydrogels were washed in ethanol three times and in deionized water three times with

sonication to remove all unreacted precursors.

In vitro antimicrobial assay of hydrogels

(1) Preparation of bacterial suspensions

Bacteria (*E. coli* 8379*, S. aureus* 29213, *K. pneumoniae* 13883, *A. baumannii* 19606*,* MRSA USA300, PA01, CR-AB and CR-PA) were inoculated and dispersed in Mueller-Hinton broth (MHB, 4 mL) at 37 °C with continuous shaking at 220 rpm to mid log phase. Bacterial suspension (1 mL) was added into a sterile microtube and MHB was removed by centrifugation, followed by decanting of the supernatant. Bacteria were washed with phosphate buffered saline (PBS, 1 mL) thrice and the final bacteria suspensions were prepared with PBS (1 mL).

(2) Inoculation of bacteria on hydrogels

Bacterial suspension in PBS (10 μL), containing approximately 1×10^7 CFU was inoculated and spread evenly onto the surface of hydrogels, which were placed on a small petri dish. A control was prepared by inoculating bacteria on a small petri dish with no hydrogel. The hydrogels were incubated at 37 °C for 1 h with 90% relative humidity.

(3) Bacterial counts

Hydrogels were immersed in PBS (1 mL) and vortexed to release bacteria. Then, a series of ten-fold dilutions of the bacterial suspensions were prepared in a 24-well plate and dilutions were plated onto Luria-Bertani (LB) agar. The plates were incubated at 37 °C for 16 h and bacterial colonies were counted.

Results were evaluated as follows (Equation 1):

Log reduction = Log (total CFU of control) – Log (total CFU on hydrogels) (1)

In vitro biocompatibility assay of hydrogels

Biocompatibility studies were carried out on human dermal fibroblasts (NHDF-Ad-Der Fibroblasts, CC2511, Lonza). Fully supplemented DMEM, consisting of fetal bovine serum (FBS, 10%) and antibiotics (penicillin-streptomycin, 1%) was used as cell culture medium.

(1) Transwell MTT assay

HDF cells were cultured in 24-well plates from an initial density of 5×10^4 cells in each well, and incubated in a CO_2 incubator at 37 °C for 24 h for cell attachment. Hydrogels were placed in transwell inserts (Falcon, 1 μm pores) before incubation with HDF cells at 37 °C for 24 h. Then, the hydrogels were removed and the culture media were replaced with MTT solution (1 mg mL^{-1} in DMEM) and incubated at 37 °C for 4 h to stain viable cells. MTT solution was discarded, dimethylsulfoxide (DMSO) was added and mixed well. The cell viability was calculated based on the absorbance of each well at 570 nm against the cell only control wells which served as the 100% cell viability control.

Results were evaluated as follows (Equation 2):

$$Cell\ viability\ (\%) = \frac{Absorbance\ of\ hydrogel\ treated\ cells}{Absorbance\ of\ control\ cells} \times 100\% \quad (2)$$

(2) Contact MTT assay

The procedures are same as Transwell MTT assay, but hydrogels were immersed in the cell cultures directly instead of transwell inserts.

Swelling kinetics of hydrogels

Hydrogels were washed thoroughly and lyophilized to dryness. The mass of fully dried hydrogels were weighed at time zero. Then, copious amount of deionized water was added to the hydrogels to induce swelling. The mass of the swelled hydrogels were taken at 5, 10, 15, 20, 25 and 30 min after drying with filter paper. Swelling ratio was calculated using the formula (Equation 3):

$$Swelling\ ratio = \frac{mass\ of\ hydrogel\ at\ n^{th}\ min - initial\ mass\ of\ hydrogel}{initial\ mass\ of\ hydrogel} \quad (3)$$

LIVE/DEAD staining to examine bacterial viability and membrane permeabilization

Suspensions of bacteria (MRSA USA300 and PA01, 1×10^9 CFU mL^{-1}) in PBS were prepared followed by inoculation (10 µL, bacterial count = 1×10^7 CFU) on the hydrogels, after which they were incubated at 37 ºC for 1 h. Then, the hydrogels were stained with BacLight bacterial viability kit L13152 reagents (Invitrogen) for 15 min at room temperature. The hydrogels were then imaged at surfaces inoculated with bacteria with confocal microscopy (ZEISS LSM 800). A control was prepared by staining live bacteria on PEGDMA hydrogel.

Scanning electron microscopy to visualize hydrogel-bacteria interactions

Suspensions of bacteria (MRSA USA300 and PA01, 1×10^9 CFU mL^{-1}) in PBS were prepared followed by inoculation (10 µL, bacteria count = 1×10^7 CFU) on the hydrogels, after which they were incubated at 37 ºC for 1 h. Then, the bacteria were fixed on the hydrogels by dripping a small amount of glutaraldehyde. The hydrogels were then freeze dried overnight before sectioning and FE-SEM imaging using a JEOL JSM-6701 FE-SEM. A control was prepared using PEGDMA hydrogel.

Mouse *in vivo* wound infection model

(1) Wounding experiment and FACS analysis

Eight-week old female C57BL/6 mice were used. The mice were anaesthetized, depilated and two 6 mm diameter full-thickness excisional wounds were inflicted on the dorsal skin and the underlying panniculus carnosus as previously described.[36] Next, bacteria (MRSA USA300 and PA01, 1×10^6 CFU in 20 μL of PBS) were topically inoculated onto the wounds and left to settle for 10 min prior to application of the dressing to simulate an infection that is promptly treated. Hydrogels were applied on the wounds and secured with Tegaderm (3M) transparent dressing. Untreated infected and uninfected wounds served as controls. At 3 days post injury and treatment, the wounds including 5 mm of the peripheral region were excised. Single-cell suspensions from wound samples were obtained using gentleMACS Dissociator according to the manufacturer's protocol (Miltenyi Biotec). Cells were immuno-labelled with CD11b and Ly6G (Biolegends) and flow cytometry was carried out using an Accuri C6 flow cytometer (BD Biosciences). Data analysis was performed using Flowjo software version 7.6.5 (Tree Star). The mean percentage values (n = 6) were plotted for each treatment, ± SEM. A two-tailed Student's t test was used for comparisons. All animal studies were approved and performed in compliance with the regulations of the Institutional Animal Care and Use Committee of Nanyang Technological University.

(2) Infection models and enumeration of bacterial load on wounded skin

Wound creation and infection procedures are the same as above. Bacteria tested were MRSA USA300, CR-AB, CR-PA and PA01. Treatments were applied 24 h post-infection. In the 24 h treatment study, dressings were removed after 24 h and the wounds, including 5 mm of the

peripheral region, were excised. In the 7-day study, wounds were harvested on days 1, 3, 5 and 7. Each wound was homogenized in PBS (900 μL) to release bacteria (n = 6). Then, a series of ten-fold dilutions of bacterial suspension was done in PBS and plated on LB agar. The plates were incubated at 37 °C for 16 h and bacterial colonies were counted. A two-tailed Student's t test was used for comparisons.

(3) Full wound healing study

PEI(1a) hydrogel and MRSA USA300 bacteria were used for this study. At day 0, mice were wounded and infected with bacteria. The wounding and infection procedures are the same as above. Untreated wounds were secured with Tegaderm and served as controls, while PEI(1a) hydrogels were applied to the treated wounds and were secured with Tegaderm. Photographs of the wounds were taken before dressing application and on days 1, 3, 5, 7, 9, 12 and 14, and at these points the dressings were replaced with fresh hydrogels. The wound size at each time point was determined using ImageJ software (n = 6). A two-tailed Student's t test was used for comparisons. Wound sizes were calculated using the formula (Equation 4):

$$Wound\ size\ (\%) = \frac{wound\ area\ on\ n^{th}\ day}{wound\ area\ on\ day\ 0} \times 100\% \quad (4)$$

(4) Histological analysis

Wound biopsies were fixed in paraformaldehyde-PBS (PFA, 4%) overnight at 4 °C. For paraffin embedding procedure, the tissues were dehydrated over a graded series of increasing concentrations of ethanol followed by xylene. Dehydrated tissues were submerged in molten paraffin wax prior to paraffin embedding using the tissue embedding System Leica EG1160 (Leica Microsystems, USA). Paraffin sections of 5 μm thickness were used for basic Haematoxylin and Eosin staining. Images of stained sections were captured using an Axioscan

Z1 (Carl Ziess).

(5) Confocal imaging of hydrogel after treatment

mCherry tagged MRSA USA300 and GFP tagged PA01 and the 24 h post-infection treatment model were used. PEI(1a) hydrogels were retrieved after one day of treatment. The wound contact surfaces of the hydrogels were imaged by 3D confocal microscopy (ZEISS LSM800).

(6) Wound fluid incubation of fluorescent hydrogels

Wound fluid was extracted by vortexing one infected wound tissue sample in PBS (1 mL) for 10 min. PEI(1a) hydrogel was compared with acrylamide-bonded PEI(aca) hydrogel (synthesis is described in Supporting Scheme S1.1c). The PEI component of the hydrogels were tagged with rhodamine B before incubation with extracted wound fluid for 24 h. PBS was used as the control fluid. The fluorescence intensity of the solutions were measured with LS 55 fluorescence spectrometer (PerkinElmer) at excitation wavelength of 553 nm and emission wavelength of 576 nm, and subtracted with the intensity of blank wound fluid. The quantities of PEI polymer released into the system were calculated based on a standard curve done independently (Supporting Figure S3.3). A two-tailed Student's t test was used for comparison.

Acknowledgements

This work was funded and supported by a Singapore MOE Tier 3 grant (MOE2013-T3-1-002), a Singapore MOH Industry Alignment Fund (NMRC/MOHIAFCAT2/003/2014). Yeo Chun Kiat acknowledges the support of NTU through IGS-HealthTech PhD scholarship.

Author contributions

C. K. Yeo carried out the syntheses of hydrogel polymers, formation of hydrogel wound dressings, *in vitro* and *in vivo* experiments. Y. S. Vikhe helped out with some syntheses and analysis of NMR characterizations. P. Li and Z. Guo established the chemistry of hydrogel polymer syntheses and did early antimicrobial testing. P. Greenberg advised on interpretations of the antimicrobial results. H. W. Duan discussed the polymer synthesis and characterization. N. S. Tan advised on the design and interpretation of *in vivo* experiments. M. B. Chan-Park advised on the design and interpretation of all experiments, and directed the overall project. C. K. Yeo and M. B. Chan-Park did the main writing of the manuscript.

Additional information

Supporting information accompanies this paper to describe experimental methods and results that are not presented in the main paper. Correspondence and requests for materials should be addressed to M. B. Chan-Park.

References

(1) Ling, L. L.; Schneider, T.; Peoples, A. J.; Spoering, A. L.; Engels, I.; Conlon, B. P.; Mueller, A.; Schaberle, T. F.; Hughes, D. E.; Epstein, S.; Jones, M.; Lazarides, L.; Steadman, V. A.; Cohen, D. R.; Felix, C. R.; Fetterman, K. A.; Millett, W. P.; Nitti, A. G.; Zullo, A. M.; Chen, C.; Lewis, K. A new antibiotic kills pathogens without detectable resistance. *Nature* **2015,** *517* (7535), 455-9, DOI: 10.1038/nature14098.

(2) Lee, W.; Schaefer, K.; Qiao, Y.; Srisuknimit, V.; Steinmetz, H.; Muller, R.; Kahne, D.; Walker, S. The Mechanism of Action of Lysobactin. *J Am Chem Soc* **2016,** *138* (1), 100-3, DOI: 10.1021/jacs.5b11807.

(3) Draper, M. P.; Weir, S.; Macone, A.; Donatelli, J.; Trieber, C. A.; Tanaka, S. K.; Levy, S. B. Mechanism of action of the novel aminomethylcycline antibiotic omadacycline. *Antimicrob Agents Chemother* **2014,** *58* (3), 1279-83, DOI: 10.1128/AAC.01066-13.

(4) Hoerr, V.; Duggan, G. E.; Zbytnuik, L.; Poon, K. K.; Grosse, C.; Neugebauer, U.; Methling, K.; Loffler, B.; Vogel, H. J. Characterization and prediction of the mechanism of action of antibiotics through NMR metabolomics. *BMC Microbiol* **2016,** *16*, 82, DOI: 10.1186/s12866-016-0696-5.

(5) Gonzalez, J. F.; Alberts, H.; Lee, J.; Doolittle, L.; Gunn, J. S. Biofilm Formation Protects Salmonella from the Antibiotic Ciprofloxacin In Vitro and In Vivo in the Mouse Model of chronic Carriage. *Sci Rep* **2018,** *8* (1), 222, DOI: 10.1038/s41598-017-18516-2.

(6) Olsen, I. Biofilm-specific antibiotic tolerance and resistance. *Eur J Clin Microbiol Infect Dis* **2015,** *34* (5), 877-86, DOI: 10.1007/s10096-015-2323-z.

(7) Hall, C. W.; Mah, T. F. Molecular mechanisms of biofilm-based antibiotic resistance and tolerance in pathogenic bacteria. *FEMS Microbiol Rev* **2017,** *41* (3), 276-301, DOI: 10.1093/femsre/fux010.

(8) Lebeaux, D.; Ghigo, J. M.; Beloin, C. Biofilm-related infections: bridging the gap between clinical management and fundamental aspects of recalcitrance toward antibiotics. *Microbiol Mol Biol Rev* **2014,** *78* (3), 510-43, DOI: 10.1128/MMBR.00013-14.

(9) de la Fuente-Nunez, C.; Reffuveille, F.; Fernandez, L.; Hancock, R. E. Bacterial biofilm development as a multicellular adaptation: antibiotic resistance and new therapeutic strategies. *Curr Opin Microbiol* **2013,** *16* (5), 580-9, DOI: 10.1016/j.mib.2013.06.013.

(10) Funao, H.; Nagai, S.; Sasaki, A.; Hoshikawa, T.; Tsuji, T.; Okada, Y.; Koyasu, S.; Toyama, Y.; Nakamura, M.; Aizawa, M.; Matsumoto, M.; Ishii, K. A novel hydroxyapatite film coated with ionic silver via inositol hexaphosphate chelation prevents implant-associated infection. *Sci Rep* **2016,** *6*, 23238, DOI: 10.1038/srep23238.

(11) GhavamiNejad, A.; Park, C. H.; Kim, C. S. In Situ Synthesis of Antimicrobial Silver Nanoparticles within Antifouling Zwitterionic Hydrogels by Catecholic Redox Chemistry for Wound Healing Application. *Biomacromolecules* **2016,** *17* (3), 1213-23, DOI: 10.1021/acs.biomac.6b00039.

(12) Wu, K.; Yang, Y.; Zhang, Y.; Deng, J.; Lin, C. Antimicrobial activity and cytocompatibility of silver nanoparticles coated catheters via a biomimetic surface functionalization strategy. *Int J Nanomedicine* **2015,** *10*, 7241-52, DOI: 10.2147/IJN.S92307.

(13) Augustine, R.; Kalarikkal, N.; Thomas, S. Electrospun PCL membranes incorporated with biosynthesized silver nanoparticles as antibacterial wound dressings. *Applied Nanoscience* **2015,** *6* (3), 337-344, DOI: 10.1007/s13204-015-0439-1.

(14) Shao, W.; Wu, J.; Wang, S.; Huang, M.; Liu, X.; Zhang, R. Construction of silver sulfadiazine loaded chitosan composite sponges as potential wound dressings. *Carbohydr Polym* **2017,** *157*, 1963-1970, DOI: 10.1016/j.carbpol.2016.11.087.

(15) Wirth, S. M.; Bertuccio, A. J.; Cao, F.; Lowry, G. V.; Tilton, R. D. Inhibition of bacterial surface colonization by

immobilized silver nanoparticles depends critically on the planktonic bacterial concentration. *J Colloid Interface Sci* **2016,** *467*, 17-27, DOI: 10.1016/j.jcis.2015.12.049.
(16) Percival, S. L.; Slone, W.; Linton, S.; Okel, T.; Corum, L.; Thomas, J. G. Use of flow cytometry to compare the antimicrobial efficacy of silver-containing wound dressings against planktonic Staphylococcus aureus and Pseudomonas aeruginosa. *Wound Repair Regen* **2011,** *19* (3), 436-41, DOI: 10.1111/j.1524-475X.2011.00685.x.
(17) Percival, S. L.; McCarty, S. M. Silver and Alginates: Role in Wound Healing and Biofilm Control. *Adv Wound Care (New Rochelle)* **2015,** *4* (7), 407-414, DOI: 10.1089/wound.2014.0541.
(18) Chen, Z.; Ji, H.; Liu, C.; Bing, W.; Wang, Z.; Qu, X. A Multinuclear Metal Complex Based DNase-Mimetic Artificial Enzyme: Matrix Cleavage for Combating Bacterial Biofilms. *Angew Chem Int Ed Engl* **2016,** *55* (36), 10732-6, DOI: 10.1002/anie.201605296.
(19) Li, P.; Poon, Y. F.; Li, W.; Zhu, H. Y.; Yeap, S. H.; Cao, Y.; Qi, X.; Zhou, C.; Lamrani, M.; Beuerman, R. W.; Kang, E. T.; Mu, Y.; Li, C. M.; Chang, M. W.; Leong, S. S.; Chan-Park, M. B. A polycationic antimicrobial and biocompatible hydrogel with microbe membrane suctioning ability. *Nat Mater* **2011,** *10* (2), 149-56, DOI: 10.1038/nmat2915.
(20) Zhou, C.; Wu, Y.; Thappeta, K. R. V.; Subramanian, J. T. L.; Pranantyo, D.; Kang, E. T.; Duan, H.; Kline, K.; Chan-Park, M. B. In Vivo Anti-Biofilm and Anti-Bacterial Non-Leachable Coating Thermally Polymerized on Cylindrical Catheter. *ACS Appl Mater Interfaces* **2017,** *9* (41), 36269-36280, DOI: 10.1021/acsami.7b07053.
(21) Irawan, H.; Yasa, K. P. A case report of diabetic foot ulcer underwent an autolytic debridement using hydrogel and hydrocellular foam combination. *Bali Med. J.* **2017,** *6* (3), S93-S96, DOI: 10.15562/bmj.v3i3.411.
(22) Dong, Y. L.; Liu, W. Q.; Lei, Y. L.; Wu, T. X.; Zhang, S. W.; Guo, Y. C.; Liu, Y.; Chen, D. M.; Yuan, Q.; Wang, Y. Y. Effect of gelatin sponge with colloid silver on bone healing in infected cranial defects. *Mater. Sci. Eng. C-Mater. Biol. Appl.* **2017,** *70*, 371-377, DOI: 10.1016/j.msec.2016.09.015.
(23) Soehnlein, O.; Steffens, S.; Hidalgo, A.; Weber, C. Neutrophils as protagonists and targets in chronic inflammation. *Nat Rev Immunol* **2017,** *17* (4), 248-261, DOI: 10.1038/nri.2017.10.
(24) Eming, S. A.; Martin, P.; Tomic-Canic, M. Wound repair and regeneration: Mechanisms, signaling, and translation. *Science Translational Medicine* **2014,** *6* (265).
(25) Organization, W. H. WHO publishes list of bacteria for which new antibiotics are urgently needed.
(26) Kamarun, D.; Zheng, X.; Milanesi, L.; Hunter, C. A.; Krause, S. A peptide cross-linked polyacrylamide hydrogel for the detection of human neutrophil elastase. *Electrochimica Acta* **2009,** *54* (22), 4985-4990, DOI: 10.1016/j.electacta.2009.03.067.
(27) Wu, D.; Gao, Y.; Li, W.; Zheng, X.; Chen, Y.; Wang, Q. Selective Adsorption of La3+ Using a Tough Alginate-Clay-Poly(n-isopropylacrylamide) Hydrogel with Hierarchical Pores and Reversible Re-Deswelling/Swelling Cycles. *ACS Sustainable Chemistry & Engineering* **2016,** *4* (12), 6732-6743, DOI: 10.1021/acssuschemeng.6b01691.
(28) Kazemi, F.; Mohamadnia, Z.; Kaboudin, B.; Gharibi, H.; Ahmadinejad, E.; Taran, Z. Synthesis, characterization and swelling behavior investigation of hydrogel based on AAm and AA using CdS nanorods as photocatalyst initiator under different irradiations. *Journal of Photochemistry and Photobiology A: Chemistry* **2016,** *330*, 102-109, DOI: 10.1016/j.jphotochem.2016.07.022.
(29) Cuetos, A.; Patti, A. Equivalence of Brownian dynamics and dynamic Monte Carlo simulations in multicomponent colloidal suspensions. *Phys Rev E Stat Nonlin Soft Matter Phys* **2015,** *92* (2), 022302, DOI: 10.1103/PhysRevE.92.022302.
(30) Hisatake, K.; Tanaka, S.; Aizawa, Y. Evaporation rate of water in a vessel. *Journal of Applied Physics* **1993,** *73* (11), 7395-7401, DOI: 10.1063/1.354031.
(31) Souliotis, K.; Kalemikerakis, I.; Saridi, M.; Papageorgiou, M.; Kalokerinou, A. A cost and clinical effectiveness analysis among moist wound healing dressings versus traditional methods in home care patients with pressure ulcers. *Wound Repair Regen* **2016,** *24* (3), 596-601, DOI: 10.1111/wrr.12433.

(32) Basu, P.; Kumar, U. N.; Manjubala, I. Wound healing materials – a perspective for skin tissue engineering. *Current Science* **2017,** *112* (12), 2392-2404.
(33) Hackl, F.; Kiwanuka, E.; Philip, J.; Gerner, P.; Aflaki, P.; Diaz-Siso, J. R.; Sisk, G.; Caterson, E. J.; Junker, J. P.; Eriksson, E. Moist dressing coverage supports proliferation and migration of transplanted skin micrografts in full-thickness porcine wounds. *Burns* **2014,** *40* (2), 274-80, DOI: 10.1016/j.burns.2013.06.002.
(34) Periasamy, S.; Joo, H. S.; Duong, A. C.; Bach, T. H. L.; Tan, V. Y.; Chatterjee, S. S.; Cheung, G. Y. C.; Otto, M. How Staphylococcus aureus biofilms develop their characteristic structure. *Proceedings of the National Academy of Sciences of the United States of America* **2012,** *109* (4), 1281-1286, DOI: 10.1073/pnas.1115006109.
(35) Otto, M. Phenol-soluble modulins. *Int. J. Med. Microbiol.* **2014,** *304* (2), 164-169, DOI: 10.1016/j.ijmm.2013.11.019.
(36) Tan, N. S.; Wahli, W. Studying Wound Repair in the Mouse. *Curr Protoc Mouse Biol* **2013,** *3* (3), 171-85, DOI: 10.1002/9780470942390.mo130135.

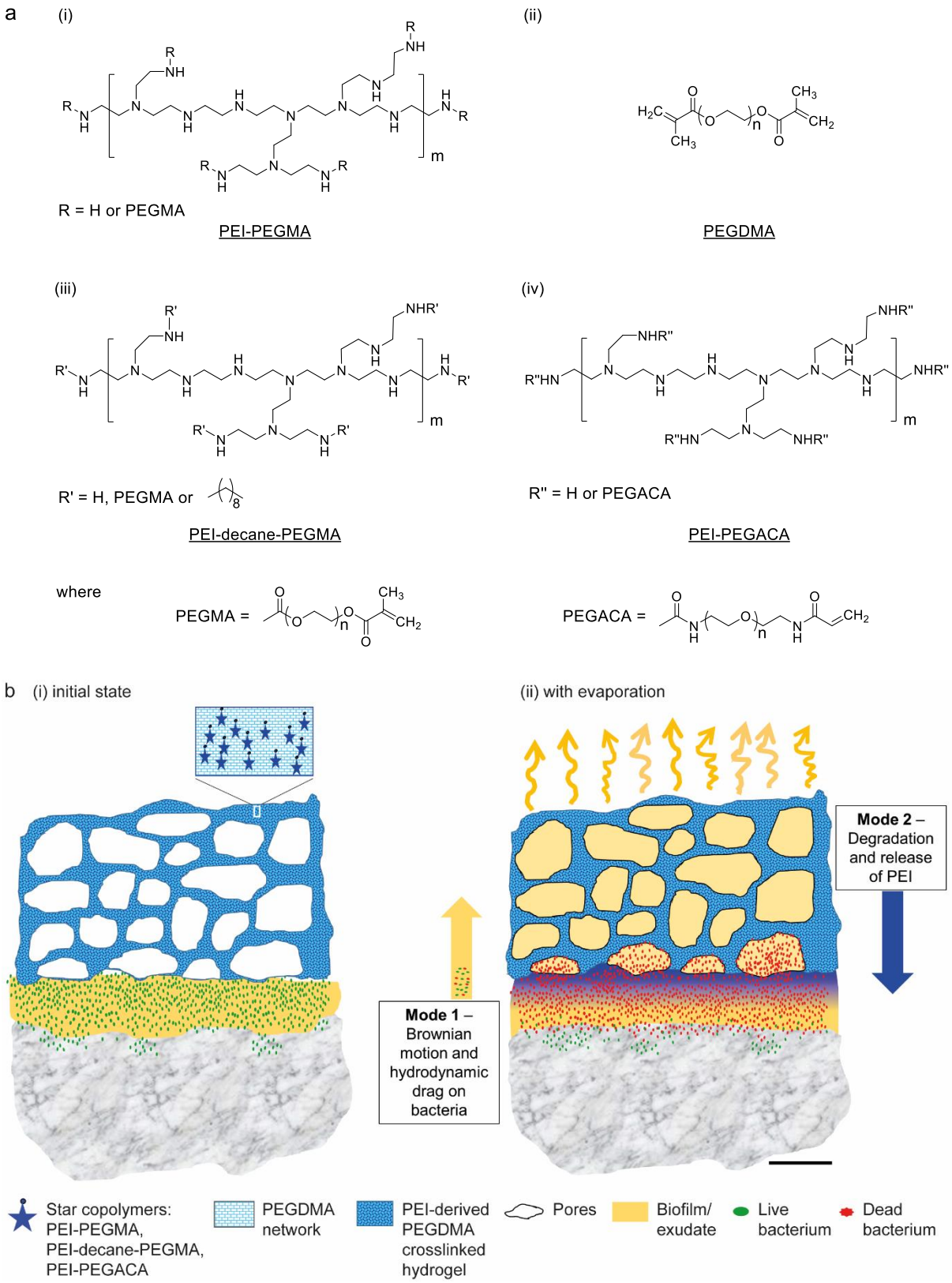

Scheme 1. Hydrogel polymers and the antibacterial killing mechanisms of their hydrogels. a) Chemical structures of (i) PEI-PEGMA (PEI(1a)); (ii) PEGDMA; (iii) PEI-decane-PEGMA (PDP); (iv) PEI-PEGACA (PEI(aca)) polymers. b) Schematic diagram showing the killing mechanisms of the biofilm-debridement and infection-degradable antibacterial hydrogel. Biofilm bacteria are killed and removed by

absorption into the hydrogel followed by contact-killing (mode 1) and infection-triggered release of bactericidal star cationic PEI (mode 2). Scale bar on the right is 20 μm.

Table 1. Characteristics and log reductions of different formulations of PEI hydrogels against eight strains of bacteria.

Hydrogel Series		1a	1b	1c	1d	1e	2	3	4
Short forms		PEI(1a)							PDP
1) Composition	**Weight %**								
a. Cationic polymer	10%	PEI(25K)-PEGMA (1:1)	PEI(25K)-PEGMA (1:2)	PEI(25K)-PEGMA (1:3)	PEI(25K)-PEGMA (1:4)	PEI(25K)-PEGMA (1:6)	PEI(800)-PEGMA (1:1)	PEI(750K)-PEGMA (1:6)	PEI(25K)-decane-PEGMA (1:10:2)
b. Crosslinker	10%	PEGDMA	PEGDMA	PEGDMA	PEGDMA	PEGDMA	PEGDMA	PEGDMA	PEGDMA
2) Grafting ratio		**PEGMA per PEI molecule (mole/mole)**							
	Design	1	2	3	4	6	1	6	2
	Actual	1.25	1.83	3.02	4.24	5.96	0.9	6.50	2.08
3) Hydrogel Bactericidal activity	**Bacteria**	**Bacterial log reduction**							
	PA01	7.31*	6.37	5.55	4.49	3.39	0.23	7.31*	7.31*
	CR-PA	7.63*	6.33	5.12	4.90	3.87	0.87	7.63*	7.63*
	A. baumannii 19606	7.55*	6.10	5.60	4.73	3.38	0.68	7.55*	7.55*
	CR-AB	7.33*	6.23	5.84	5.31	4.39	0.82	7.33*	7.33*
	E. coli 8739	7.12*	6.72	5.52	4.34	3.93	1.45	7.12*	7.12*
	K. pneumoniae 13883	7.13*	6.35	5.55	4.24	3.34	0.77	7.13*	7.13*
	S. aureus 29213	7.35*	7.35*	7.35*	5.48	4.28	2.56	7.35*	7.35*
	MRSA USA300	7.52*	7.52*	7.52*	5.39	4.27	0.45	7.52*	7.52*

* denotes that no bacterial colonies were observed on the agar plate after incubation for 16 h. The initial bacterial inoculum was approximately 1 x 10^7 CFU per sample. PEGDMA is polyethylene glycol dimethacrylate.

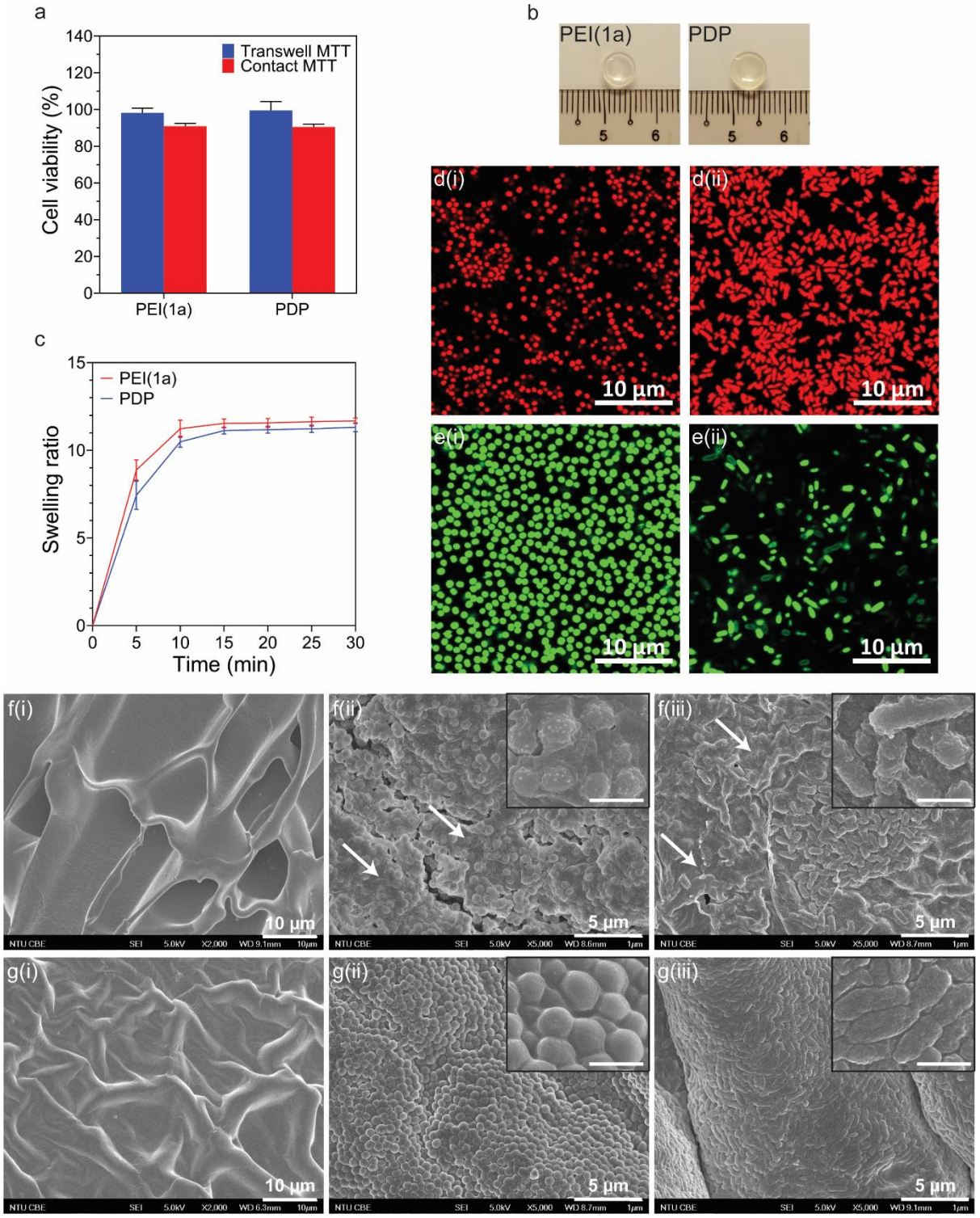

Figure 1. ***In vitro*** **characterizations of hydrogels, morphologies and viability of bacteria in hydrogels.** a) Cell viability of human dermal fibroblasts (HDF) when incubated with PEI(1a) and PDP hydrogels for 24 h with Transwell and contact MTT assays (n=3). b) Photos of 6 mm circular disc of PEI(1a) and PDP hydrogel with scale reference. c) Swelling ratio (final mass/initial mass) against time of PEI(1a) and PDP hydrogels (n=3). d) Confocal images of (i) MRSA USA300 and (ii) PA01 on PEI(1a) hydrogel surface using LIVE/DEAD assay. e) Confocal images of (i) MRSA USA300 and (ii) PA01 on control (PEGDMA) hydrogel surface using LIVE/DEAD assay. Incubation time for bacteria on hydrogel is 1 h. Green color indicates

viable bacteria while red color indicates dead bacteria. f) Morphology of cross-section of (i) PEI(1a) hydrogel, (ii) MRSA USA300 and (iii) PA01 on PEI(1a) hydrogel using FE-SEM. g) Morphology of cross-section of (i) control PEGDMA hydrogel, (ii) MRSA USA300 and (iii) PA01 on control hydrogel using FE-SEM. Insets show magnified morphology (scale bar = 1 μm). White arrows indicate bacteria debris.

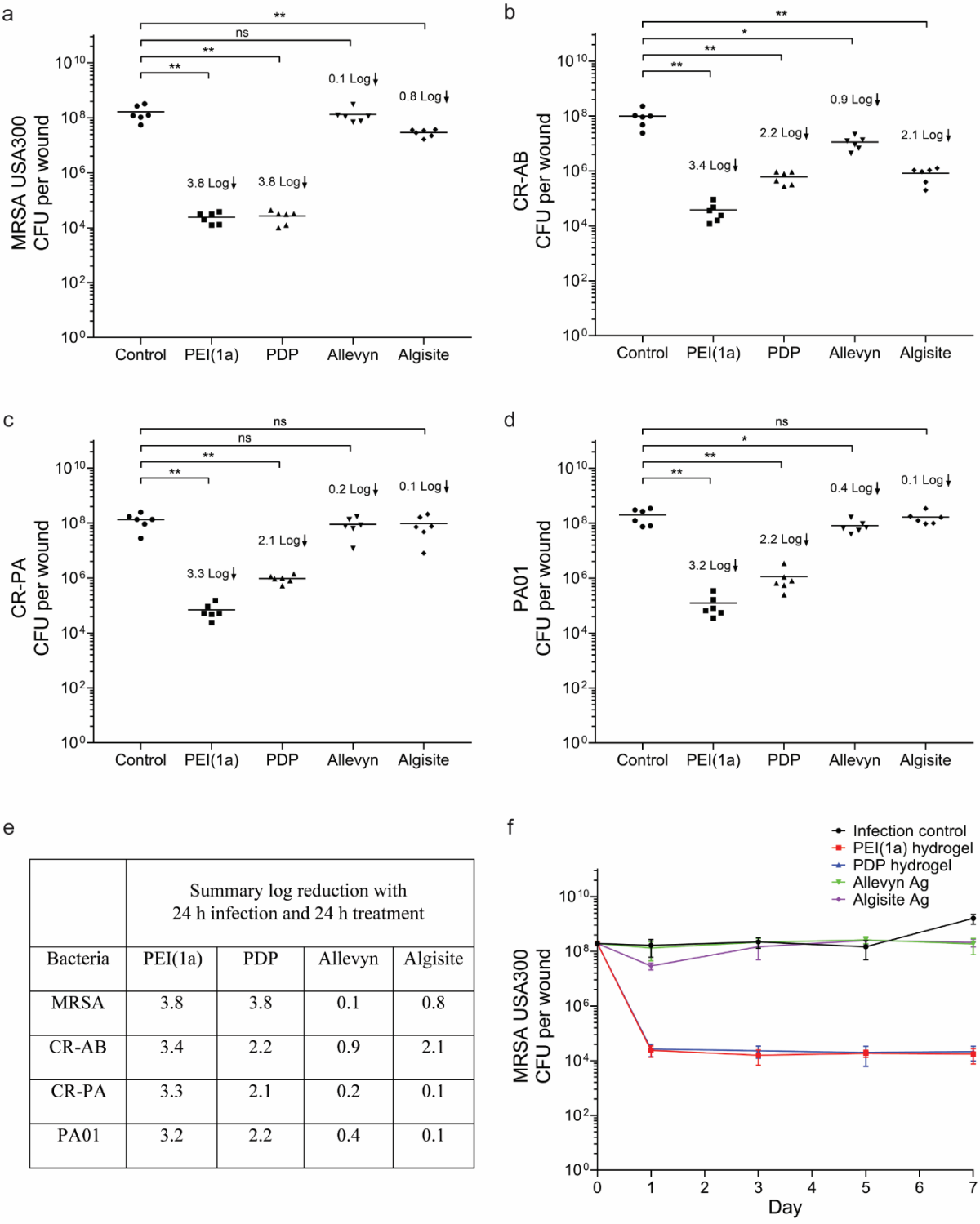

	Summary log reduction with 24 h infection and 24 h treatment			
Bacteria	PEI(1a)	PDP	Allevyn	Algisite
MRSA	3.8	3.8	0.1	0.8
CR-AB	3.4	2.2	0.9	2.1
CR-PA	3.3	2.1	0.2	0.1
PA01	3.2	2.2	0.4	0.1

Figure 2. Mouse *in vivo* wound infection model with 24 h post-infection treatment. Bacterial counts of (a) MRSA USA300, (b) CR-AB, (c) CR-PA and (d) PA01 on various treated and control wounds after one day in a 24 h post-infection treatment model (n=6). * denotes $P < 0.05$ and ** denotes $P < 0.01$. e) Table summarizing the log reduction data from Figures 2a-d. f) Bacterial counts of MRSA USA300 on various treated and control wounds on days 1, 3, 5 and 7 (n=6).

a

	Summary log reduction with 0+ h infection and 24 h treatment			
Bacteria	PEI(1a)	PDP	Allevyn	Algisite
MRSA	4.3	4.2	0.8	2.9
CR-AB	4.0	3.7	1.9	2.0
CR-PA	4.1	3.9	2.1	3.5
PA01	4.1	3.9	3.1	3.8

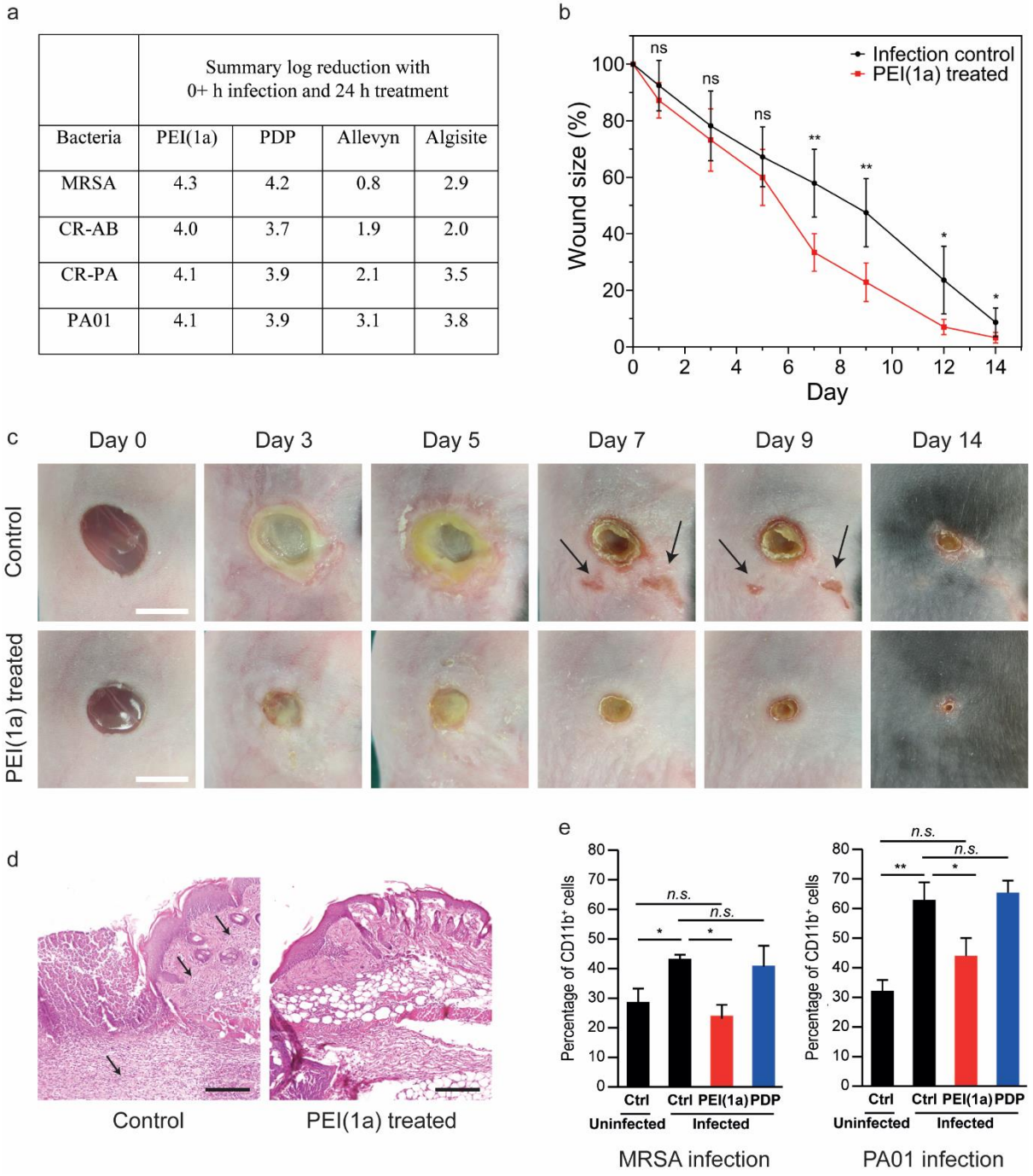

Figure 3. Full wound healing study for the *in vivo* prophylactic model. a) Table summarizing the log reduction data for 0^+ h post-infection treatment model (full data can be found in Supporting Figures S3.1a-d). b) Wound sizes of infection control and PEI(1a) hydrogel treated wounds on various days as a percentage of the initial wound size (n=6). c) Wound pictures of infection control and PEI(1a) hydrogel treated wounds on various days. Scale bar = 5 mm. Black arrows indicate secondary infection sites. d) H&E stains of the tissues beside the wound bed showing the extent of inflammation in wounds of infection control and PEI(1a) hydrogel treated wounds on day 3. Black arrows signify inflamed areas as indicated by dark spots. Scale bar = 300 µm. e) Percentage of $CD11b^+$ cells on wounds after treatment for 3 days with MRSA USA300 and PA01 infected mice (n=6). The percentage of $CD11b^+$ cells is directly proportional to the extent of inflammation in the skin. * denotes $P < 0.05$ and ** denotes $P < 0.01$.

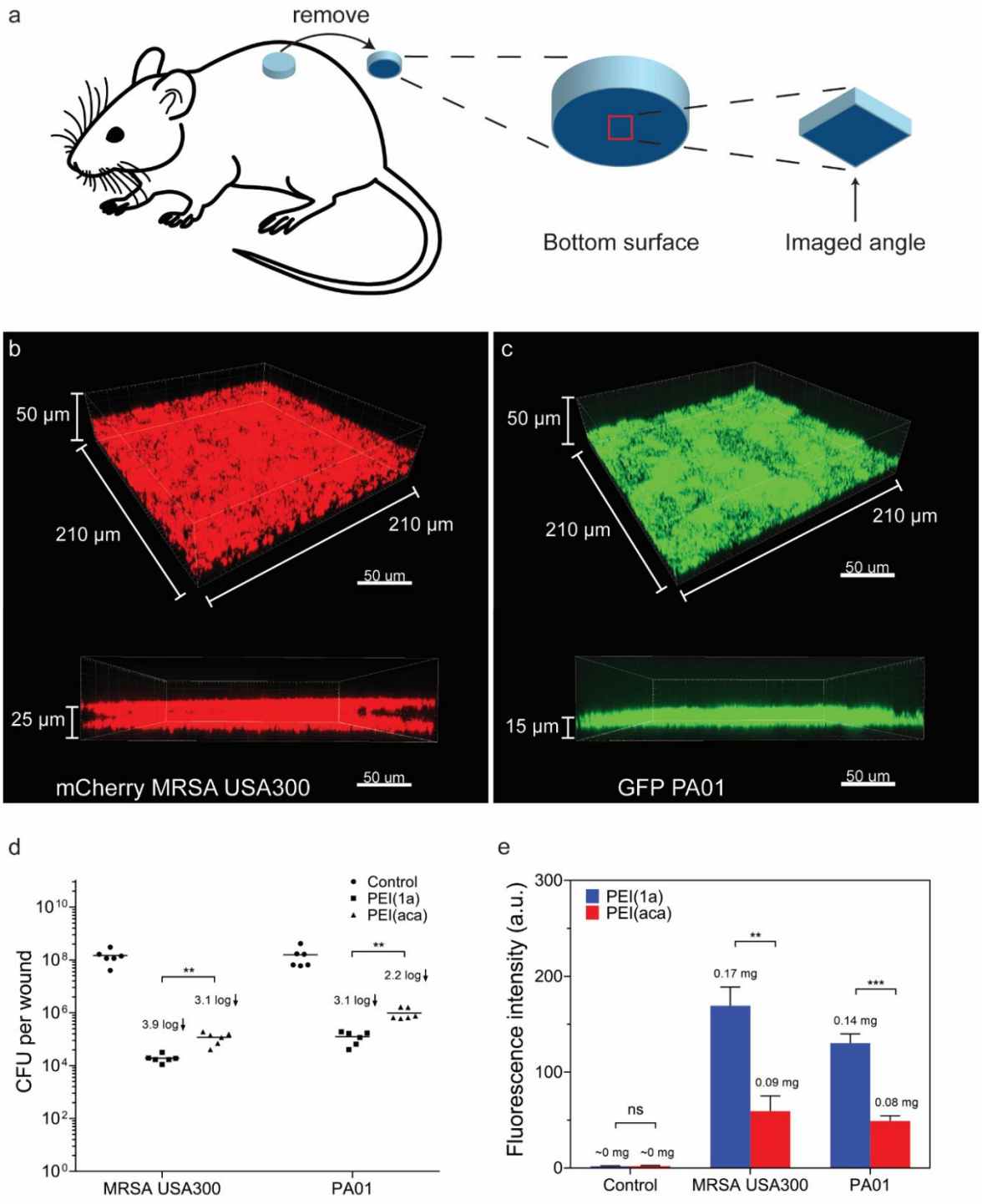

Figure 4. Killing mechanisms of the hydrogel. a) Schematic showing the imaged angle of the hydrogel for confocal microscopy. b-c) 3D and side views of the (b) mCherry MRSA USA300 and (c) GFP PA01 trapped in the bottom (wound contact) surface of the PEI(1a) hydrogel. d) The bacterial counts of MRSA USA300 and PA01 on PEI(1a) and PEI(aca) hydrogel treated wounds after one day in a 24 h post-infection treatment model (n=6). e) The fluorescence intensities of 1 mL of extracted wound fluid from MRSA USA300 and PA01 infected wounds immersed with rhodamine B labelled PEI(1a) and PEI(aca) hydrogel. Control was done by immersing hydrogels in PBS. The amount of fluorescent PEI released into the solution was calculated based on a standard curve (Supporting Figure S3.3) measured independently and is indicated above each bar (n=3). ** denotes $P < 0.01$ and *** denotes $P < 0.001$.

TOC

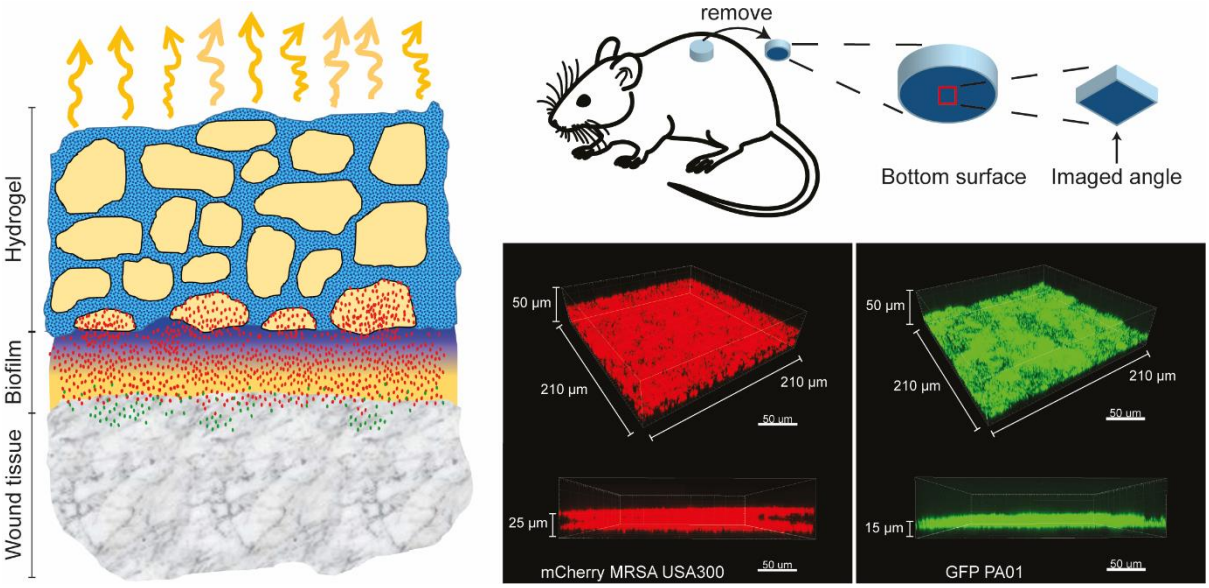
Hydrogel
Biofilm
Wound tissue
remove
Bottom surface
Imaged angle
50 μm
210 μm
210 μm
50 μm
25 μm
mCherry MRSA USA300
50 μm
210 μm
210 μm
50 μm
15 μm
GFP PA01
50 μm

Supporting Information

Hydrogel effects rapid biofilm debridement with *ex-situ* contact-kill to eliminate multi-drug resistant bacteria *in vivo*

Chun Kiat Yeo[1,2], Yogesh Shankar Vikhe[2,3], Peng Li[2], Zanru Guo[2], Peter Greenberg[4], Hongwei Duan[2,3], Nguan Soon Tan[5]*, Mary B. Chan-Park*[2,3]

[1]NTU Institute for Health Technologies, Interdisciplinary Graduate School, Nanyang Technological University, Singapore 637553

[2]School of Chemical and Biomedical Engineering, Nanyang Technological University, 62 Nanyang Drive, Singapore 637459

[3]Centre for Antimicrobial Bioengineering, Nanyang Technological University, Singapore 637459

[4]Department of Microbiology, University of Washington School of Medicine, Seattle, Washington, 98195-7735, USA

[5]School of Biological Sciences, Nanyang Technological University, Singapore 637551

*E-mail: mbechan@ntu.edu.sg; NSTan@ntu.edu.sg

Supporting Information

This supporting section contains all experimental methods and results that were not presented in the main paper.

S1: Synthesis and characterization of hydrogel polymers

Preparation of chloro-functionalized polyethylene glycol methacrylate (Cl-PEGMA)

Polyethylene glycol methacrylate (PEGMA, M_n = 360) (11.8 mL, 35.3 mmol) was first dissolved in toluene (100 mL), then chloroacetyl chloride (11.25 mL, 141.2 mmol) was added into the solution at room temperature. The solution was stirred and refluxed for 24 h, then cooled and toluene was evaporated on a rotary evaporator. The gum was dissolved in methylene chloride (100 mL), then potassium carbonate (1 g) was added to the solution and the mixture was stirred for 10 min. Then, the solid potassium carbonate was removed by filtration and solvent evaporation afforded the desired Cl-PEGMA (Scheme S1.1a). The product was confirmed by ^{1}H NMR (300MHz) (Figure S1.2b) in $CDCl_3$ at 25 °C: δ_H (ppm) 6.06 (m, 1H, methylene), 5.50 (m, 1H, methylene), 4.29-4.21 (m, 2H -CH_2-), 4.03 (d, 2H), 3.69-3.67 (m, 2H), 3.66-3.57 (m, ethylene protons), 1.89-1.87 (m, 3H methacrylate -CH_3-).

Preparation of polyethylenimine grafted with PEGMA (PEI-PEGMA)

Polyethylenimine (PEI) of molecular weights 800, 25,000 and 750,000 were grafted with various ratios of PEGMA. Here, we use PEI(25K)-PEGMA (1:1) as a representative example

(Scheme S1.1a). PEI (1 g) was first dissolved in deionized water (10 mL), and NaOH (0.4 mL, 1 M) solution was added at room temperature. Then, Cl-PEGMA (0.2 g) in isopropanol (1 mL) was added dropwise into the solution. The mixture was stirred for 3 h at room temperature and then subjected to dialysis (MWCO 12000-14000) in DI water for three days. The product was obtained via lyophilization. ^{1}H NMR (300MHz) (Figure S1.2c) in D_2O at 25 °C: δ_H (ppm) 5.54 (d, 1H, methylene), 5.24 (d, 1H, methylene), 3.59-3.11 (m, ethylene glycol protons), 2.80-2.57 (m, PEI ethylene protons), 1.79-1.75 (m, 3H methacrylate -CH_3-), 1.03 (m, PEI NH/NH_2 protons).

Preparation of alkylated polyethylenimine (PEI-decane)

Polyethylenimine-decane (M_w = 25,000) was prepared through alkylation reaction. PEI (2.0 g, 0.2 mmol) was dissolved in absolute ethanol (50 mL) and 1-Bromodecane (0.442 g, 2 mmol) was added at room temperature. The solution was stirred and refluxed for 24 h, then the generated HBr was neutralized with sodium hydroxide (0.2 g) under the same conditions for an additional 24 h. After removal of the solvent on rotary evaporator, the resulting residue was dissolved in DI water and dialyzed (MWCO 12000-14000) against deionized water for three days. The polymer PEI-decane was obtained via lyophilization. ^{1}H NMR (300MHz) (Figure S1.3a) in D_2O at 25 °C: δ_H (ppm) 3.05 (t, methylene -NH-CH_2- protons), 2.64-2.56 (m, PEI ethylene protons), 1.21 (m, PEI NH/NH_2 protons), 1.40-0.81 (m, decyl -CH_2-CH_3- protons).

Preparation of PEI-decane grafted with PEGMA (PEI-decane-PEGMA)

PEI-decane (1 g) was first dissolved in deionized water (10 mL) and NaOH solution (0.4 mL,

1 M) was added at room temperature. Then, Cl-PEGMA (0.64 g) in isopropanol (1 mL) was added dropwise into the solution. The mixture was stirred for 3 h at room temperature and then subjected to dialysis (MWCO 12000-14000) in DI water for three days. The polymer PEI-decane-PEGMA (Scheme S1.1b) was obtained via lyophilization. ^{1}H NMR (300MHz) (Figure S1.3b) in D_2O, 25 °C: δ_H (ppm) 5.56 (d, 1H, methylene), 5.27 (d, 1H, methylene), 3.60-3.11 (m, ethylene glycol protons), 3.01-2.58 (m, PEI ethylene protons), 1.79-1.75 (m, 3H methacrylate -CH_3-), 1.20 (m, PEI NH/NH_2 protons), 1.50-0.80 (m, decyl -CH_2-CH_3- protons).

Determination of double bond content

Double bond content was characterized according to a previous protocol with slight modifications.[19] To a solution of PEI derivative (0.06 g) in deionized water (2 mL), mercaptoethanol solution (1 mL, 3%) and NaOH solution (0.2 mL, 2 M) were added at room temperature. After stirring for 20 min and the sequential addition of HCl (0.5 mL, 1 M) and three drops of starch indicator, the solution was then titrated with iodine solution (0.05 M) until a blue coloration was observed.

The content of double bond was derived from the relation (Equation S1):

$$Double\ bond\ amount\ (mmol/g) = \frac{(V_1 - V_2) \times 0.05}{W} \quad \text{(S1)}$$

where W refers to the weight in grams of the dried methacrylated PEI derivatives, V_1 refers to the volume in mL of iodine used in titration without PEI derivative and V_2 refers to the volume in mL of iodine used for sample titration. 0.05 refers to the iodine concentration.

Results

The reaction scheme of PEI-PEGMA and chemical structure of PEI-decane-PEGMA are shown in Schemes S1.1a and S1.1b respectively. A third copolymer of PEI-PEGACA was synthesized (Scheme S1.1c) by replacing PEGMA with polyethylene glycol acrylamide (PEGACA) with the same synthesis procedures as PEI-PEGMA, to make a more stable acrylamide-bonded hydrogel to be test *in vivo*. ^{1}H NMR of the polymers are shown in Figures S1.2 and S1.3. The doublets at 5.56 ppm and 5.27 ppm are due to the methylene protons in the methacrylate group, indicating that PEGMA was successfully grafted onto PEI and PEI-decane to form PEI-PEGMA and PEI-decane-PEGMA respectively. The protons at 1.50~0.8 ppm are due to decane indicating that PEI-decane-PEGMA was successfully made. The actual grafting ratios of the PEGMA to PEI backbone were measured via titration of double bond content. The mole of PEGMA per mole of PEI were 1.25, 1.83, 3.02, 4.24, 5.96, 0.90 and 6.50 for polymers 1a – 1e, 2 and 3 respectively, and 2.08 for PEI-decane-PEGMA.

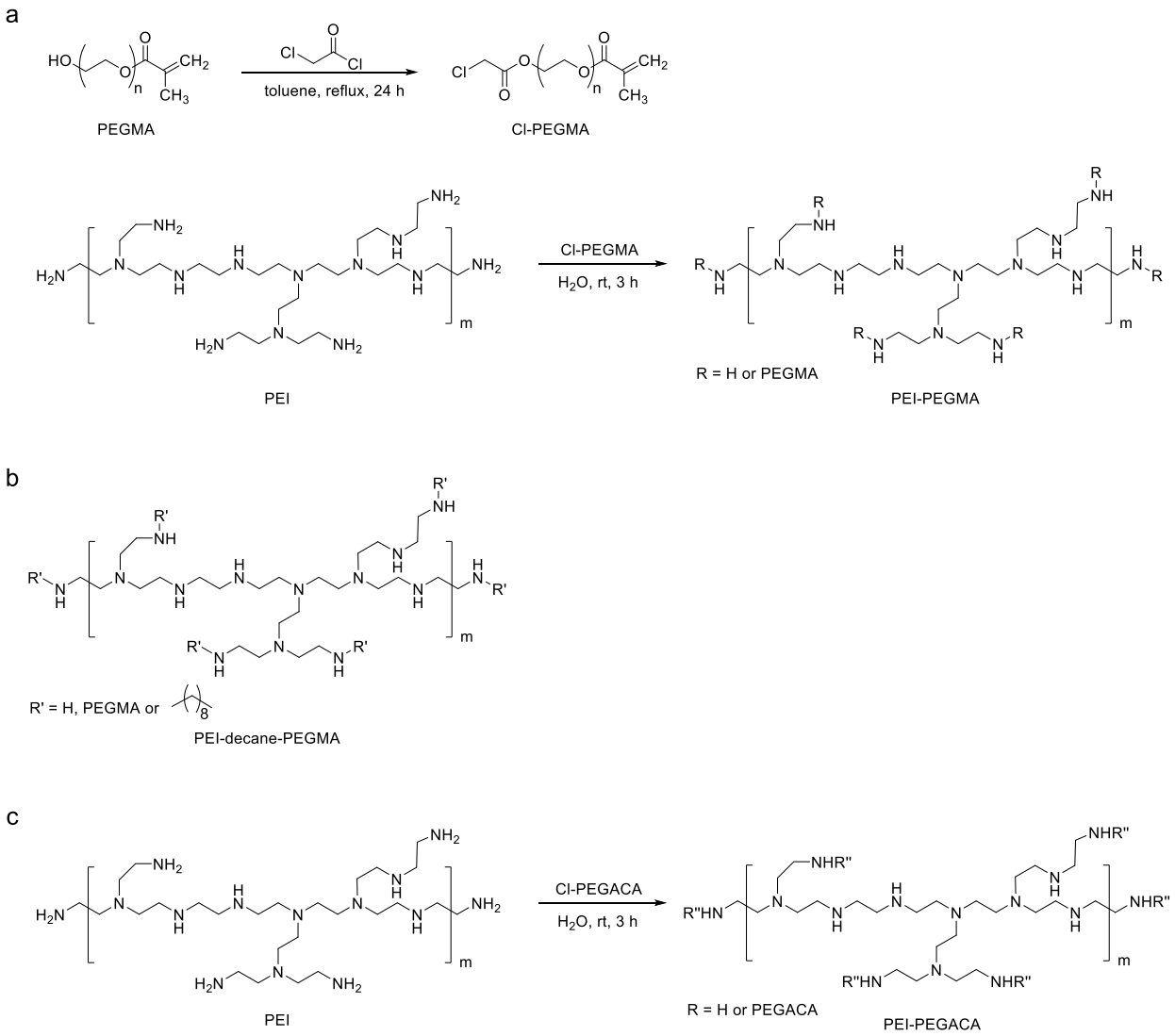

Scheme S1.1 The synthesis strategies for a) Cl-PEGMA and PEI-PEGMA; chemical structure of b) PEI-decane-PEGMA. c) PEI-PEGACA was synthesized with the same procedures as PEI-PEGMA by replacing PEGMA with PEGACA.

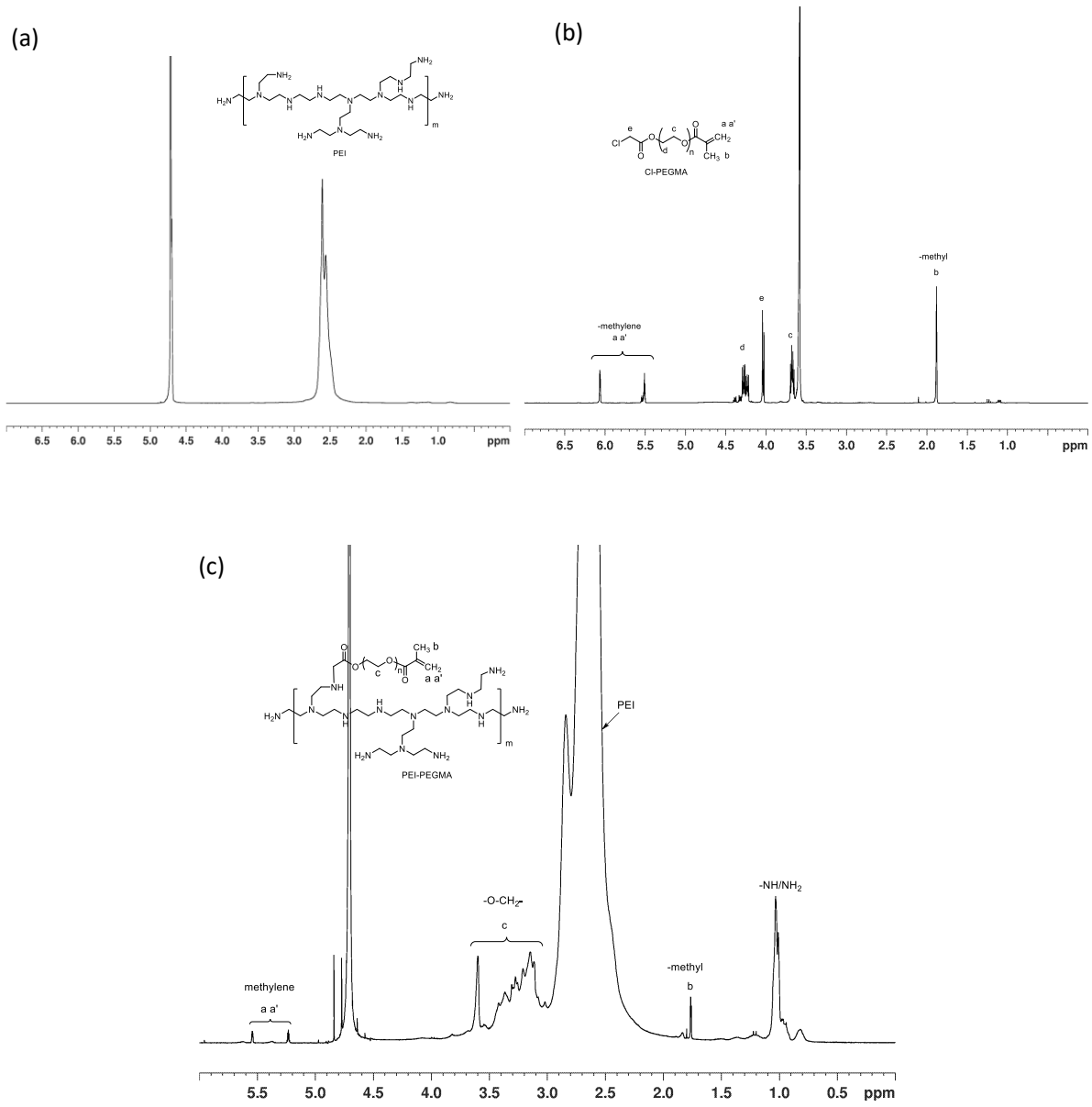

Figure S1.2 Representative NMR spectra; (a) PEI in D_2O, (b) Cl-PEGMA in $CDCl_3$ and (c) PEI-PEGMA in D_2O.

(a)

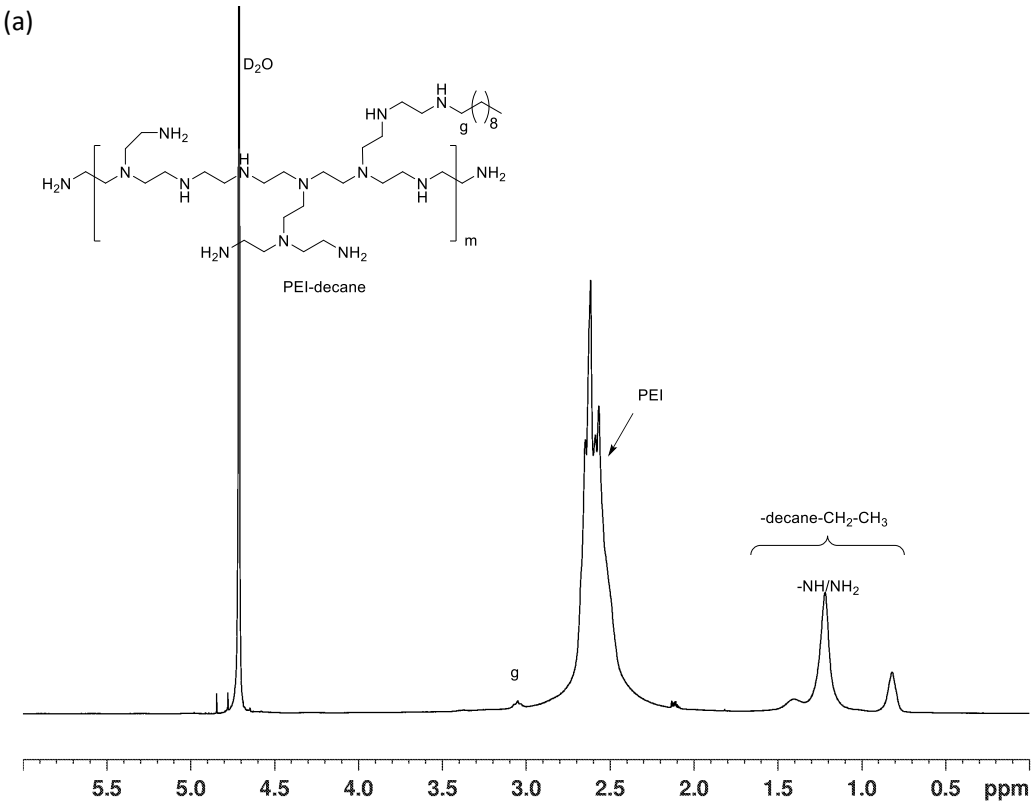
D2O
PEI-decane
PEI
-decane-CH2-CH3
-NH/NH2
g
5.5 5.0 4.5 4.0 3.5 3.0 2.5 2.0 1.5 1.0 0.5 ppm

(b)

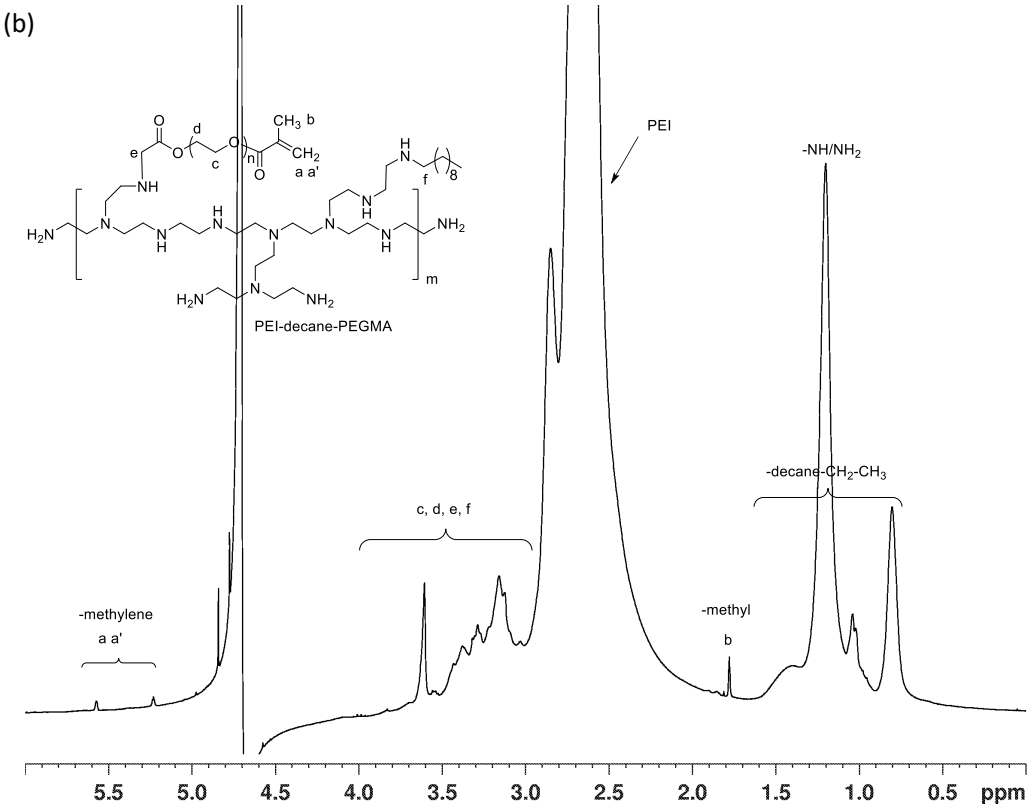
PEI-decane-PEGMA
PEI
-NH/NH2
-decane-CH2-CH3
c, d, e, f
-methylene
a a'
-methyl
b
5.5 5.0 4.5 4.0 3.5 3.0 2.5 2.0 1.5 1.0 0.5 ppm

Figure S1.3 Representative NMR spectra; (a) PEI-decane in D_2O and (b) PEI-decane-PEGMA in D_2O.

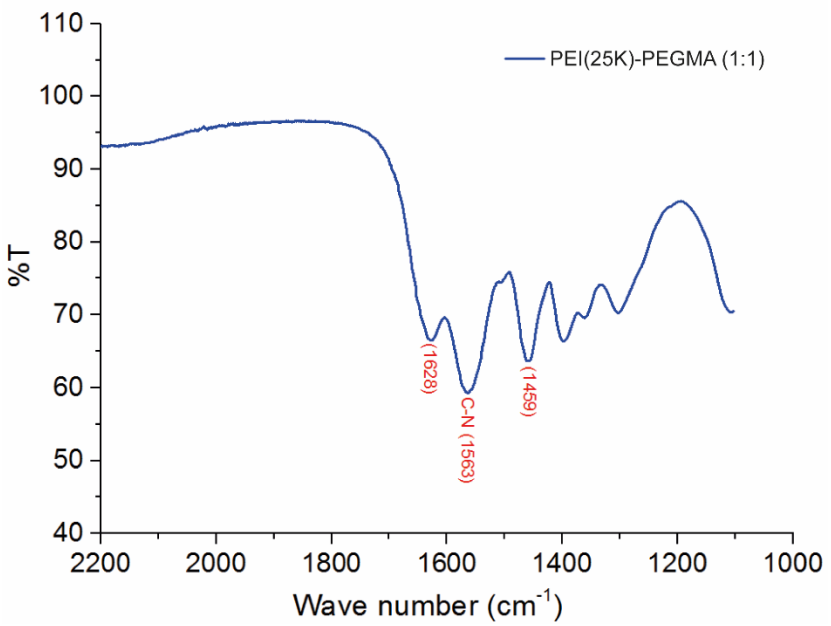

Figure S1.4 Representative FTIR spectrum of PEI(25K)-PEGMA (1:1).

S2: *In vitro* characterizations of hydrogels

Agar diffusion test

A suspension of bacteria (PA01, 1×10^9 CFU mL^{-1}) in PBS was prepared followed by spreading (100 μL) on an LB agar plate, after which they were incubated with PEGDMA (control), PEI(25K)-PEGMA (1:1) and PEI(25K)-decane-PEGMA (1:10:2) hydrogels at 37 ºC for 16 h. No zones of inhibition were observed for all of the hydrogels (Figure S2.1), proving that bacteria were killed by contact with the gels instead of leaching of residual uncured cationic polymers.

Figure S2.1 Agar diffusion test. No zones of inhibition were observed for all of the hydrogels. Control = PEGDMA hydrogel, PEI = PEI(25K)-PEGMA (1:1) hydrogel, PDP = PEI(25K)-decane-PEGMA (1:10:2) hydrogel.

Hydrogel leaching tests

Hydrogels were washed thoroughly with ethanol and water. The washed hydrogels were then immersed in deionized water (5 mL) for 24 h before measuring the UV-Vis absorbance of the solution using Thermo Evolution 600 BB UV-Vis spectrophotometer. Control was done by measuring the UV-Vis absorbance of the respective polymers at 100, 10 and 1 μg mL^{-1} concentration. Wavelengths measured were 190 – 300 nm. The amount of leachate from the post-washed hydrogels as measured by UV-Vis spectrophotometry was negligible (Figure S2.2).

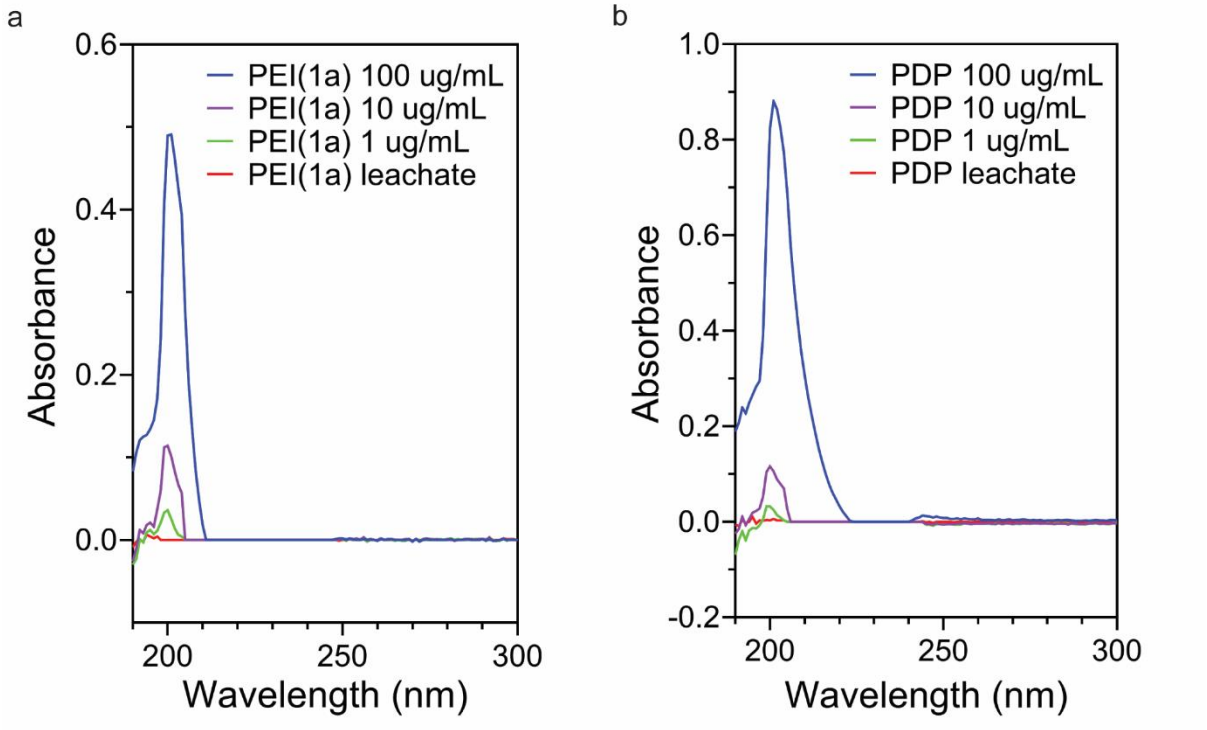

Figure S2.2 The leachability of (a) PEI(1a) hydrogel and (b) PDP hydrogel in water when compared against low concentrations of their respective raw polymers.

Compression test

The mechanical properties of the hydrogels were characterized by compressive stress–strain measurements which were performed on water-equilibrated hydrogels using an Instron 5543 Single Column Testing System. The cylindrical gel sample, 6 mm in diameter and 2 mm in thickness, was put on the lower plate and compressed by the upper plate, which was connected to a load cell, at a strain rate of 0.1 mm min^{-1}. Four parallel samples per measurement were performed, and the obtained values were averaged and plotted in a graph. The hydrogels have relatively good compressive strengths at 50% strain of 119±6.9 kPa and 12.3±1.1 kPa respectively for PEI(1a) and PDP hydrogels and also good ultimate compression strains of more than 50% (Figure S2.3).

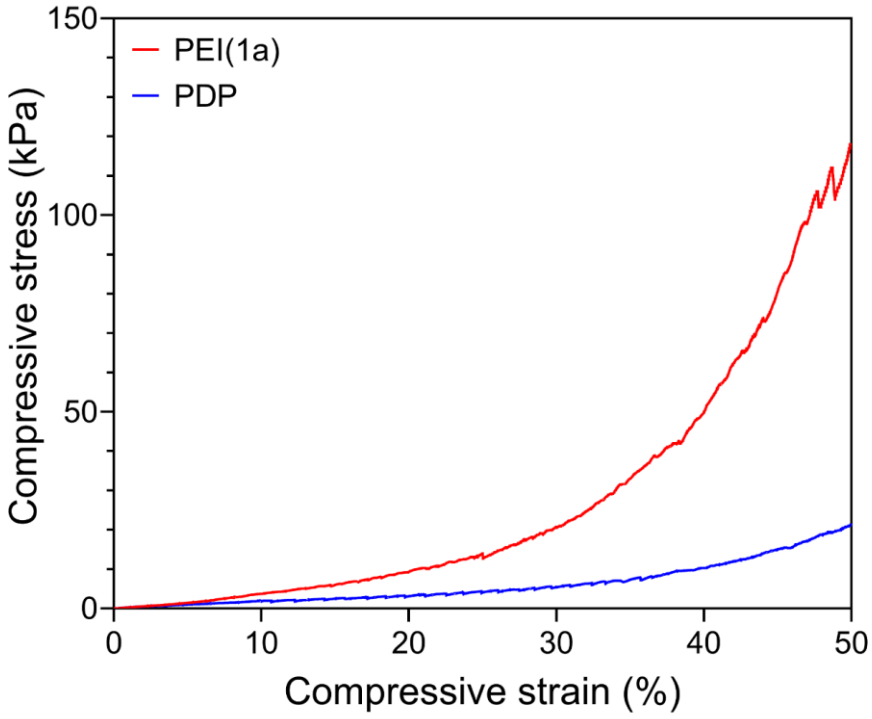

Figure S2.3 Compressive strength of hydrogels (n=4).

Contact angle measurements

Contact angles of water on hydrogels were taken with FTA200 Contact Angle Analyzer. Briefly, water was injected (20 μL min^{-1}) onto the surface of fully swollen hydrogels, until a drop of water sits on the surface of the hydrogels. The images were taken with a camera and the contact angle was measured by the accompanying software. The contact angles of water on PEI(1a) hydrogel after 0 min and 2 min of water droplet deposition were measured to be 21.8°±2.1° and 11.4°±1.2° respectively while those of PDP hydrogel were higher (50.6°±3.1° and 30.6°±2.4° respectively, Figure S2.4), corroborating that the decane graft increases the hydrophobicity of the hydrogel.

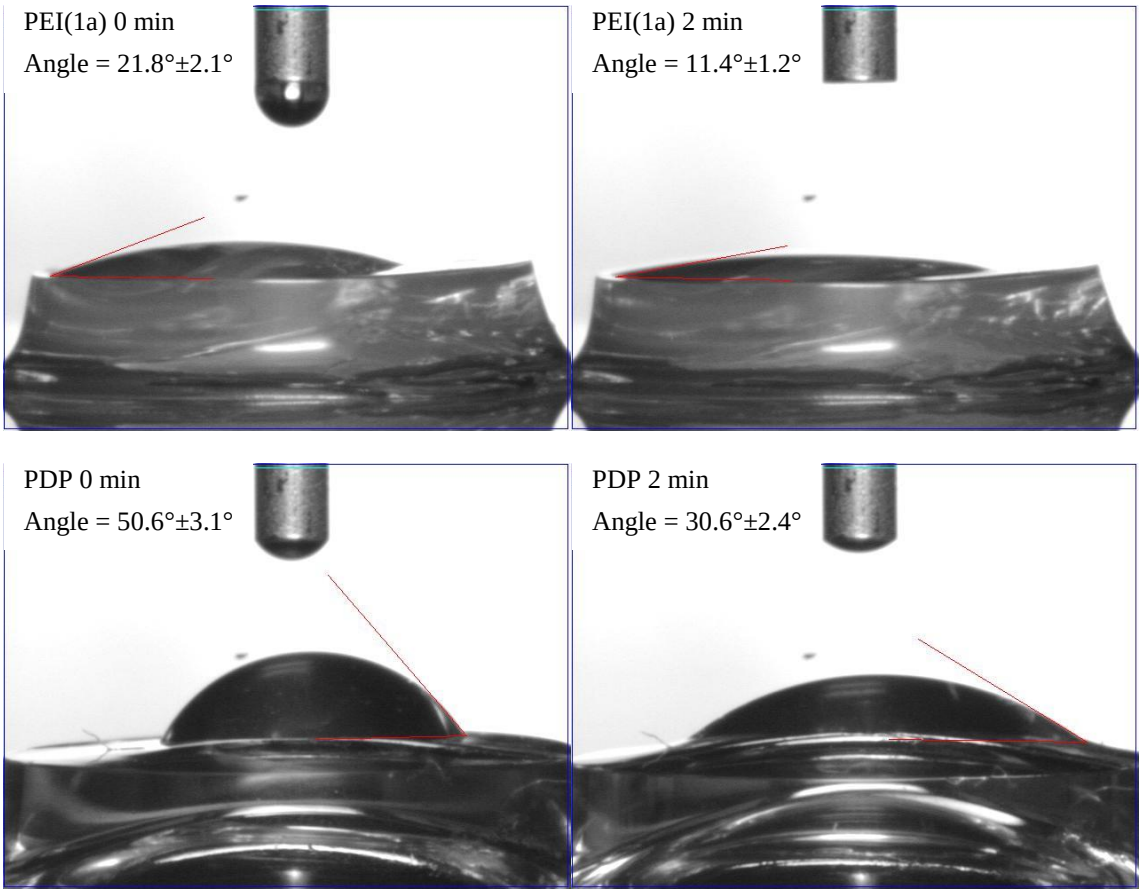

Figure S2.4 Contact angle of water on PEI(1a) and PDP hydrogels at 0 min and 2 min.

LIVE/DEAD staining to examine bacterial viability and membrane permeabilization

All bacteria inoculated on the PEI(1a) and PDP hydrogels were stained red (Figures S2.5b, c, e, f), indicating permeabilized membranes and dead bacteria. On the control hydrogel (PEGDMA), all bacteria were stained green, indicating live bacteria (Figures S2.5a, d).

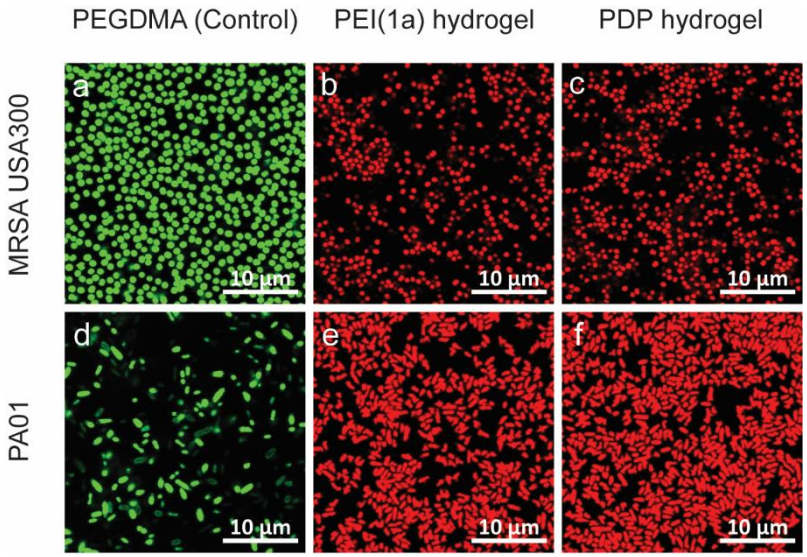

Figure S2.5 LIVE/DEAD assay on bacteria inoculated on hydrogels. a-c) Confocal images of MRSA USA300 on (a) PEDGMA control hydrogel, (b) PEI(1a) hydrogel and (c) PDP hydrogel. e-f) Confocal images of PA01 on (d) PEDGMA control hydrogel, (e) PEI(1a) hydrogel and (f) PDP hydrogel. Incubation time for bacteria on hydrogel is 1 h. Green color indicates viable bacteria while red color indicates dead bacteria.

Scanning electron microscopy to visualize hydrogel-bacteria interactions

The hydrogels are microporous with pores larger than 10 μm (Figures S2.6a, d, g). SEM of PEI(1a) and PDP hydrogels inoculated with MRSA USA300 (Figures S2.6e, h) and PA01 (Figures S2.6f, i) shows that the bacteria attach to the pore walls and experience severe membrane perturbation. Bacterial debris can also be seen sticking to the hydrogel wall (Figures S2.6e, f, h, i, arrows), likely because of cell lysis and release of cellular contents. The control hydrogel (PEGDMA) does not appear to affect the morphology of the bacteria and their membranes remain intact (Figures S2.6b, c).

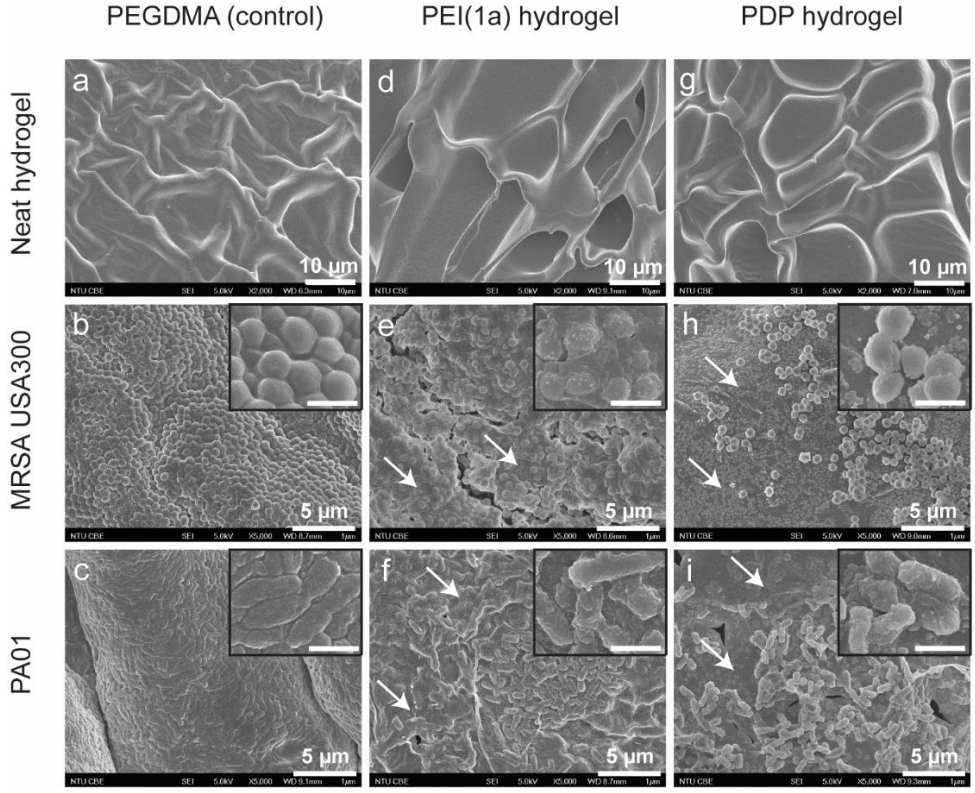

Figure S2.6 Morphology of cross-section of (a) control PEGDMA hydrogel, (b) MRSA USA300 and (c) PA01 on control hydrogel using FE-SEM. Morphology of cross-section of (d) PEI(1a) hydrogel, (e) MRSA USA300 and (f) PA01 on PEI(1a) hydrogel using FE-SEM. Morphology of cross-section of (g) PDP hydrogel, (i) MRSA USA300 and (i) PA01 on PDP hydrogel using FE-SEM. Insets show magnified morphology (scale bar = 1 μm). White arrows represent bacteria debris.

Sol content of hydrogels

Hydrogel precursor solutions were irradiated with UV light for various time points (2, 4, 6, 8, 10 min) to crosslink. Then, hydrogels were freeze dried overnight and measured for their dry mass. The hydrogels were then washed thoroughly with ethanol and water and freeze dried overnight again before measuring for their dry mass after washing. The sol content of hydrogels were calculated using the formula as follows (Equation S2).

$$Sol\ content\ (\%) = \frac{initial\ dry\ mass - dry\ mass\ after\ washing}{initial\ dry\ mass} \quad \text{(S2)}$$

The sol content data (Figure S2.7) by the ethanol/water extraction depends on UV irradiation time and beyond 8 min of UV time, Series 1 has a plateaued sol content of ~11 – 17% depending on the PEGMA grafting ratio. A higher PEGMA grafting decreased the sol content as higher crosslinking occurs.

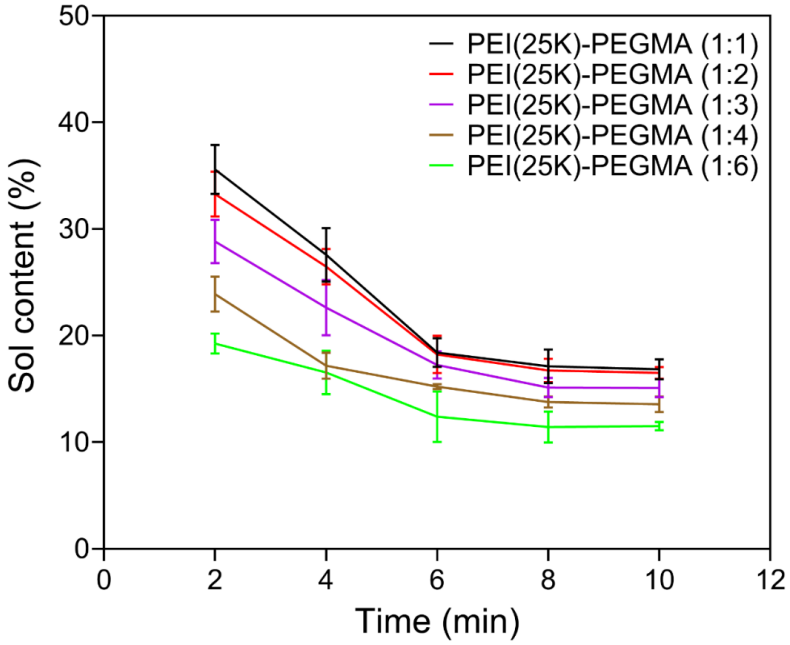

Figure S2.7 Sol content of hydrogels for the PEI(25K)-PEGMA series (n=3).

***In vitro* biocompatibility of hydrogel polymers**

In vitro biocompatibility of hydrogel polymers was tested using the same protocol as the main paper, with the exception of adding different concentration of hydrogel polymers (100 and 200 μg mL^{-1}) into the cell culture instead of hydrogels. Hydrogel polymers were relatively non-toxic at the released concentration described in the main paper.

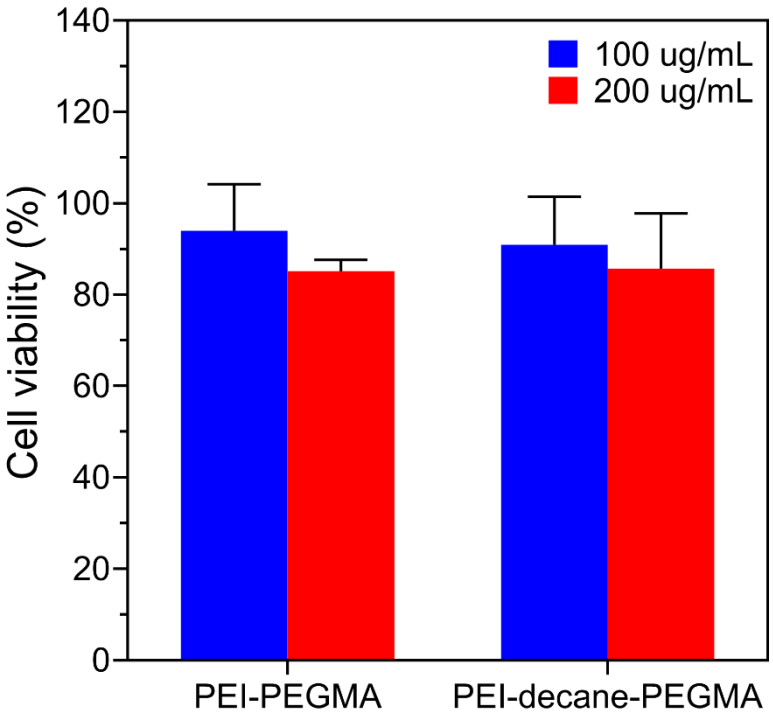

Figure S2.8 *In vitro* biocompatibility of hydrogel polymers against human dermal fibroblasts.

S3: *In vivo* antibacterial efficacy and wound healing

Mouse *in vivo* wound infection model (prophylactic treatment)

(1) Enumeration of bacteria load on wounded skin

Wound creation and infection procedures are the same as described in the main paper, except that the wound is treated immediately after infection. PEI(1a) hydrogel achieved 4.3 log reduction (>99.99%), 4.0 log reduction (>99.99%), 4.1 log reduction (>99.99%) and 4.1 log reduction (>99.99%) for MRSA USA300, CR-AB, CR-PA and PA01 respectively (Figures S3.1a-d). These bactericidal effects were better than the two commercial silver-based antibacterial wound dressings tested with an average of 2 log reduction for Allevyn Ag and 3 log reduction for Algisite Ag. We also studied the dynamics of bacteria reduction at the wound site over seven days with MRSA USA300 with the various treatments. Most of the bacterial killing occurred during the first to third days of the treatment, after which the bacteria count remained almost constant throughout the rest of the days (Figure S3.1e).

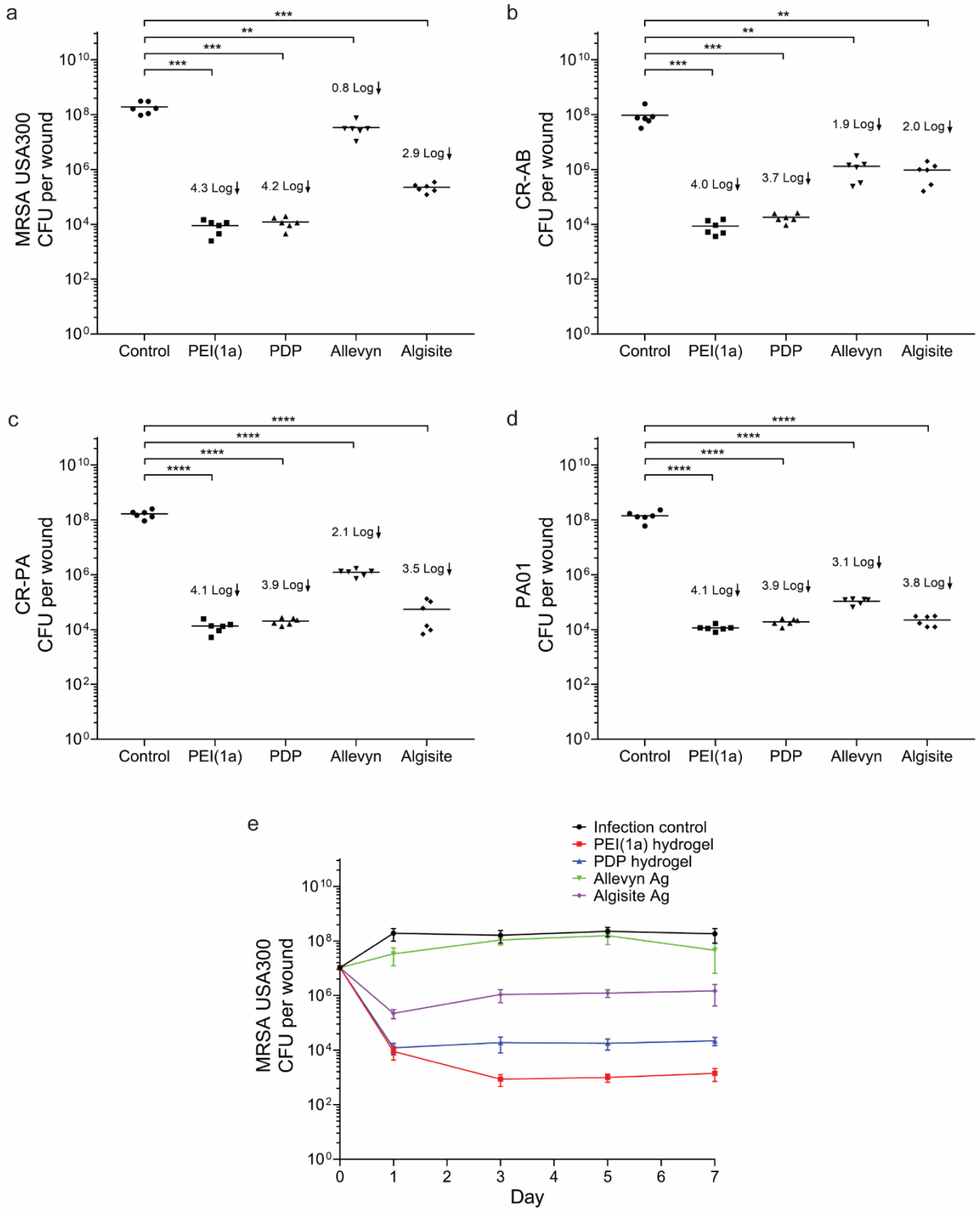

Figure S3.1 Mouse *in vivo* wound infection model with 0^+ h post-infection treatment. Bacteria counts of (a) MRSA USA300, (b) CR-AB, (c) CR-PA and (d) PA01 on various treated and control wounds after one day in a 0^+ h post-infection treatment model (n=6). *denotes $P < 0.05$ and ** denotes $P < 0.01$. e) Bacterial counts of MRSA USA300 on various treated and control wounds on days 1, 3, 5 and 7 (n=6).

Degradability of hydrogels in the presence of bacteria and macrophages

PEI(1a) hydrogels were tagged with rhodamine B and immersed in 1 mL of PBS (control), MHB media containing 1 × 10^7 CFU of either MRSA USA300 or PA01, or RPMI media containing THP-1 activated macrophages for 12 h and 24 h. The fluorescence intensity of the solutions were measured with LS 55 fluorescence spectrometer (PerkinElmer) at excitation wavelength of 553 nm and emission wavelength of 576 nm, and subtracted with blank MHB and RPMI media respectively. The quantities of PEI polymer released into the system were calculated based on a standard curve (Figure S3.3). MRSA USA300 led to more (0.33 mg) release of PEI from the hydrogel than PA01 (0.18 mg) after 24 h. The THP-1 macrophage also caused substantial release of PEI (0.35 mg) after 24 h (Figure S3.2). The longer duration shows higher release. This release of PEI polymer into the system is due to the enzymes secreted by bacteria and leukocytes (specifically lipase and esterase) that degrade the ester bonds that are formed during the hydrogel crosslinking process. Also, MRSA USA300 caused more PEI polymer to be released into the system as compared to PA01, which explained the higher order killing of MRSA USA300 in the *in vivo* experiments.

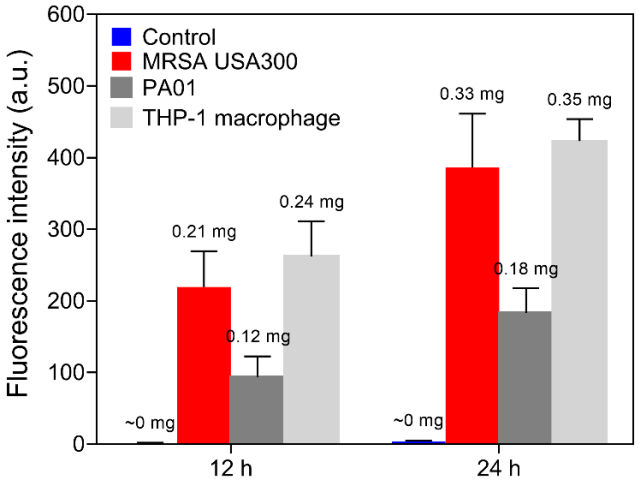

Figure S3.2 The amount of PEI polymer released into the system as a function of fluorescence intensity when incubated with different cells (n=3).

Standard curve to determine fluorescent hydrogel polymer content

Rhodamine B labelled PEI polymers were measured for their fluorescence intensity at concentrations of 1, 0.8, 0.6, 0.4, 0.2, 0.1, 0.08, 0.06, 0.04 and 0.02 mg mL^{-1} with LS 55 fluorescence spectrometer (PerkinElmer) at excitation wavelength of 553 nm and emission wavelength of 576 nm. A standard curve was plotted based on the relationship of fluorescence intensity against concentration of polymer (Figure S3.3).

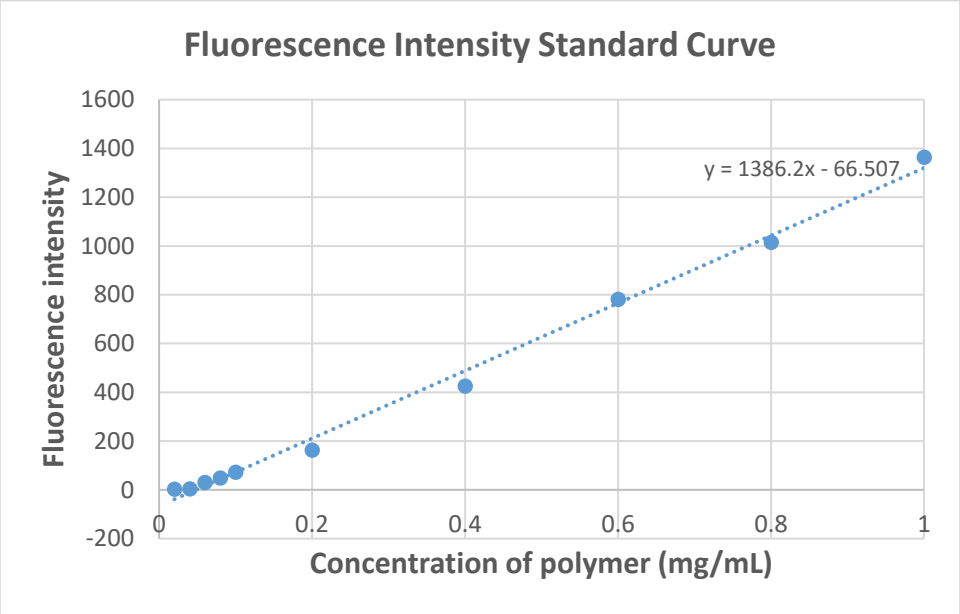

Figure S3.3 Standard curve of fluorescence intensity against concentration of PEI polymer.

(2) FACS analysis

Analysis by fluorescence-activated cell sorting (FACS) showed that the percentage of $CD11b^+$ cells (*i.e.* leukocytes, which include monocytes, neutrophils, granulocytes and macrophages) increased in untreated infected (by MRSA USA300 and PA01) wounds. However, infected wounds treated with PEI(1a) hydrogel did not show any excess of inflammatory ($CD11b^+$) cells over the levels present in uninfected wounds for both strains of bacteria (Figure S3.4), indicating that PEI(1a) hydrogel wound dressing likely reduces the inflammation due to infection by killing and removing bacteria from the wound site. PDP hydrogel, however, did not modulate the number of $CD11b^+$ cells after 3 days.

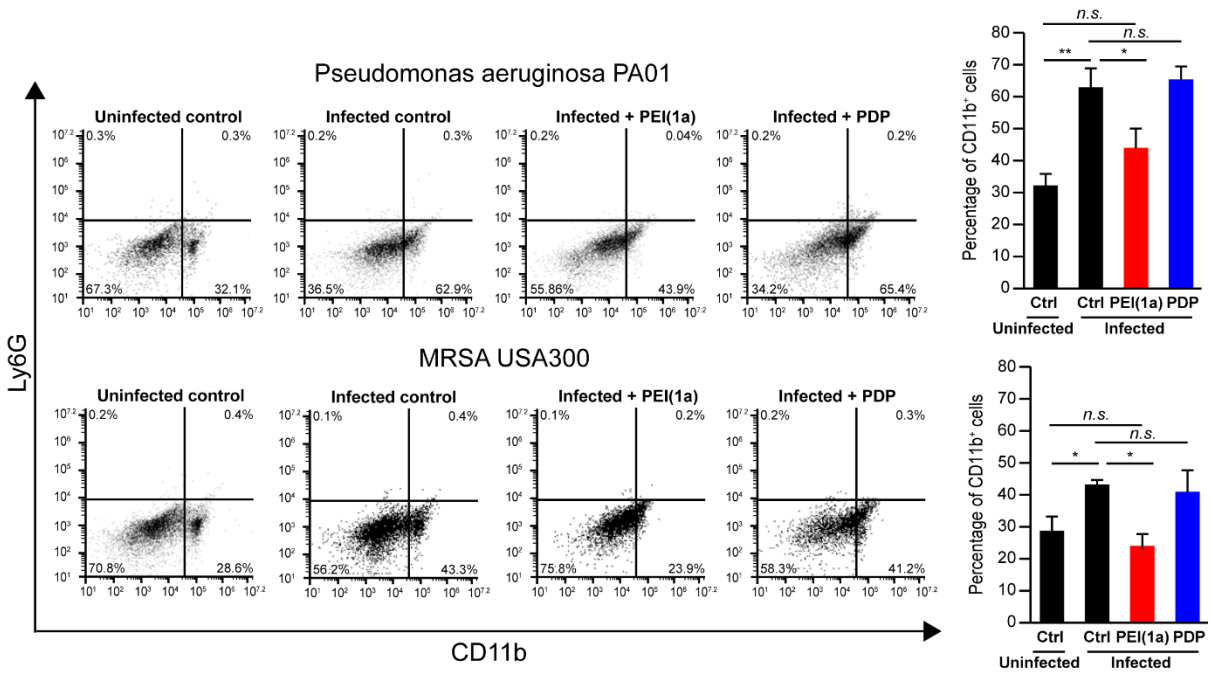

Figure S3.4 Percentage of $CD11b^+$ cells on wounds after treatment for 3 days with MRSA USA300 and PA01 infected mice (n=6). The percentage of $CD11b^+$ cells is directly proportional to the extent of inflammation in the skin. * denotes $P < 0.05$ and ** denotes $P < 0.01$.

(3) Full wound healing study

The healing of MRSA USA300 infected wounds was examined over a 2-week duration using the PEI(1a) hydrogel. At days 7, 9, 12 and 14 post-infection, the sizes (normalized to the initial wound size) of the PEI(1a) hydrogel treated wounds were much smaller than the control wounds (Figure S3.5a). Moreover, over the entire duration, the PEI(1a) hydrogel treated wounds were cleaner than the control wounds; much more pus was observed on the control wounds (Figures S3.5b, c). Furthermore, secondary wound sites were seen on the control wounds only; these were most likely caused by the spread of infection from the wound site to nearby skin areas (Figure S3.5b, arrows). A comparison among the six different control and PEI(1a) hydrogel treated wounds on day 7 showed that five out of six control wounds have secondary wound sites while none of the PEI(1a) hydrogel treated wounds have secondary wound sites (Figures S3.5b, c).

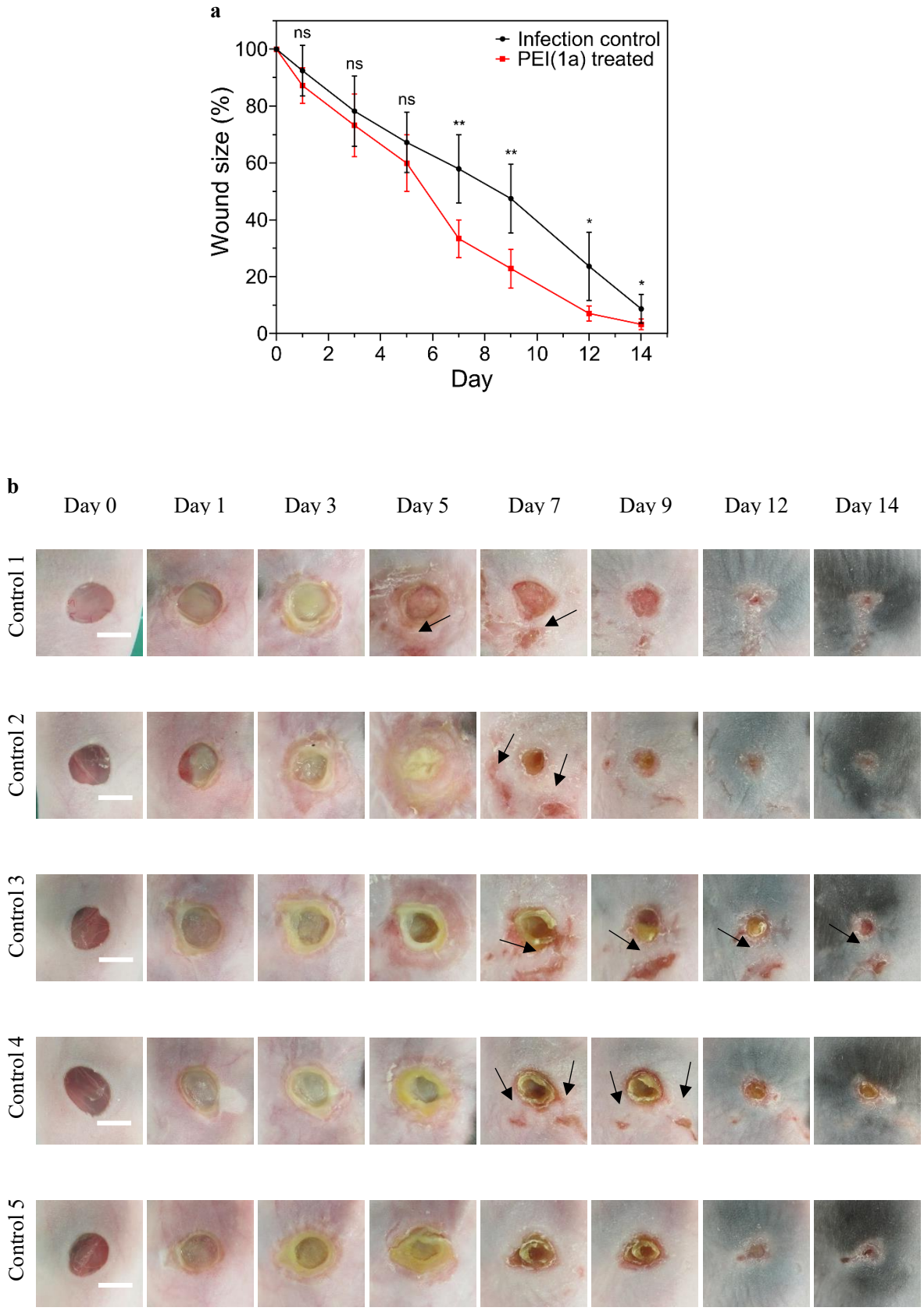
a
Infection control
PEI(1a) treated
Wound size (%)
Day
ns
ns
ns
**
**
*
*
b
Day 0
Day 1
Day 3
Day 5
Day 7
Day 9
Day 12
Day 14
Control 1
Control 2
Control 3
Control 4
Control 5

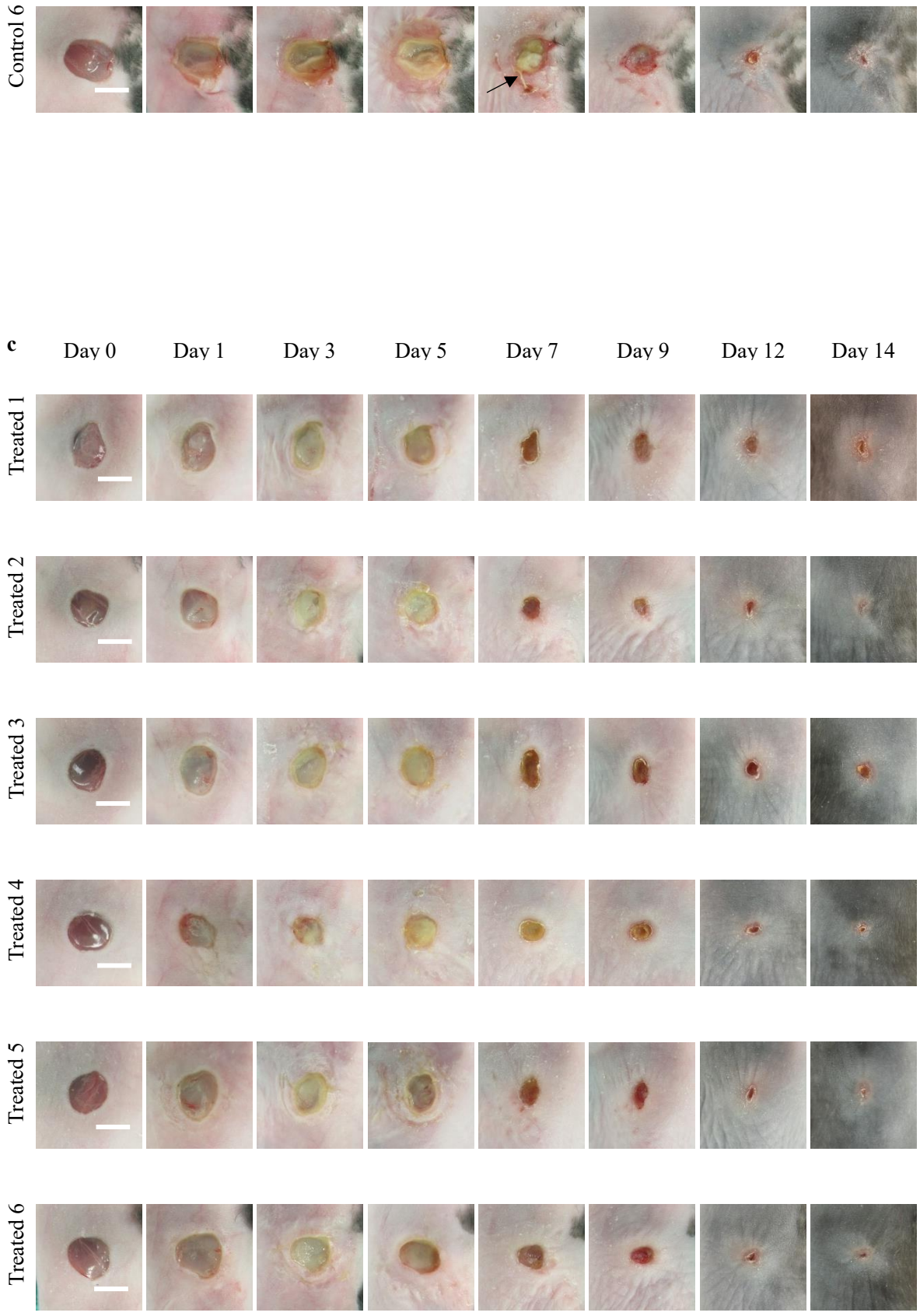
Control 6
c
Day 0
Day 1
Day 3
Day 5
Day 7
Day 9
Day 12
Day 14
Treated 1
Treated 2
Treated 3
Treated 4
Treated 5
Treated 6

Figure S3.5 Full wound healing study. a) Wound sizes of infection control and PEI(1a) hydrogel treated wounds on various days as a percentage of the initial wound size (n=6). b-c) Wound pictures of (b) infection control and (c) PEI(1a) hydrogel treated wounds on various days. Scale bar = 5 mm. Black arrows indicate secondary infection sites. * denotes $P < 0.05$ and ** denotes $P < 0.01$.

S4: Hydrodynamic drag calculation

Reynolds number

The Reynolds number is $\mathrm{Re} = \frac{V_F L}{\eta}$. Given that L is micron scale (10^{-4} cm) and V_F is of order of 10^{-4} cm s^{-1} or less and η, the dynamic viscosity, is 0.01 in the same unit system, the Reynolds number is of order 10^{-6} or less, the fluid flow is extremely laminar. The Stokes drag formula is thus highly appropriate.

Stokes Drag Formula

At low Reynolds number, the Stokes Drag Formula is appropriate:

Stoke's equation:

$$F_D = 6\pi\eta V_F R_P \tag{S3}$$

where η is the dynamic viscosity of the fluid, V_F the fluid speed with respect to the particle and R_P the spherical particle radius.

To determine the value of the fluid speed that is required to suspend a bacterium against gravity, we set the drag force equal to the differential gravitational force on the particle and its fluid environment (*i.e.*, the particle buoyant weight).

$$F_D = 6\pi\eta V_F R_P = F_G = gM_B = g\frac{4\pi R_P^3 \rho_B}{3} \tag{S4}$$

where g is the gravitational acceleration constant (g ~ 980 cm s^{-2}), M_B is the buoyant mass of the particle and ρ_B is the buoyant density of the particle, *i.e.* the difference between the mass density of the particle and the mass density of the fluid environment. It is assumed that the

particle is at least slightly denser than the fluid, otherwise it would float to the fluid surface due to buoyant forces and there would be no need for fluid drag to lift the particle against gravity. This equation may be solved for the fluid speed in terms of the other parameters of the problem:

$$V_F = \frac{2}{9}\frac{gR_P^2\rho_B}{\eta} \quad \text{(S5)}$$

The dynamic viscosity of water at room temperature is ~ 1 cP (centi-Poise, 1 cP = 0.01 g $cm^{-1}s^{-1}$) so this gives a required fluid flow of

$$V_F = 1.1\times10^{-5} cm/s\left(\frac{R_P}{0.5\mu m}\right)^2\left(\frac{\rho_B}{0.2 g/cm^3}\right) \quad \text{(S6)}$$

The diameter of MSRA from the SEM images is slightly less than 1 μm and the buoyant density of bacteria is around 0.1 g cm^{-3} [37], hence the fluid flow speed required to lift the bacteria against gravity (calculated from Equation S6) is 50 nm/s, which is about 200 μm/h. Since water evaporates at the rate of 0.722 mg/min.cm^2 at 25 °C when uncovered,[30] it can be estimated that the evaporation rate from our hydrogel (volume is 50 uL, radius is 0.32 cm) is 500 μm/h, which is higher than the flow required to lift bacteria against gravity.

References

(1) Ling, L. L.; Schneider, T.; Peoples, A. J.; Spoering, A. L.; Engels, I.; Conlon, B. P.; Mueller, A.; Schaberle, T. F.; Hughes, D. E.; Epstein, S.; Jones, M.; Lazarides, L.; Steadman, V. A.; Cohen, D. R.; Felix, C. R.; Fetterman, K. A.; Millett, W. P.; Nitti, A. G.; Zullo, A. M.; Chen, C.; Lewis, K. A new antibiotic kills pathogens without detectable resistance. *Nature* **2015,** *517* (7535), 455-9, DOI: 10.1038/nature14098.

(2) Lee, W.; Schaefer, K.; Qiao, Y.; Srisuknimit, V.; Steinmetz, H.; Muller, R.; Kahne, D.; Walker, S. The Mechanism of Action of Lysobactin. *J Am Chem Soc* **2016,** *138* (1), 100-3, DOI: 10.1021/jacs.5b11807.

(3) Draper, M. P.; Weir, S.; Macone, A.; Donatelli, J.; Trieber, C. A.; Tanaka, S. K.; Levy, S. B. Mechanism of action of the novel aminomethylcycline antibiotic omadacycline. *Antimicrob Agents Chemother* **2014,** *58* (3), 1279-83, DOI: 10.1128/AAC.01066-13.

(4) Hoerr, V.; Duggan, G. E.; Zbytnuik, L.; Poon, K. K.; Grosse, C.; Neugebauer, U.; Methling, K.; Loffler, B.; Vogel,

H. J. Characterization and prediction of the mechanism of action of antibiotics through NMR metabolomics. *BMC Microbiol* **2016,** *16*, 82, DOI: 10.1186/s12866-016-0696-5.
(5) Gonzalez, J. F.; Alberts, H.; Lee, J.; Doolittle, L.; Gunn, J. S. Biofilm Formation Protects Salmonella from the Antibiotic Ciprofloxacin In Vitro and In Vivo in the Mouse Model of chronic Carriage. *Sci Rep* **2018,** *8* (1), 222, DOI: 10.1038/s41598-017-18516-2.
(6) Olsen, I. Biofilm-specific antibiotic tolerance and resistance. *Eur J Clin Microbiol Infect Dis* **2015,** *34* (5), 877-86, DOI: 10.1007/s10096-015-2323-z.
(7) Hall, C. W.; Mah, T. F. Molecular mechanisms of biofilm-based antibiotic resistance and tolerance in pathogenic bacteria. *FEMS Microbiol Rev* **2017,** *41* (3), 276-301, DOI: 10.1093/femsre/fux010.
(8) Lebeaux, D.; Ghigo, J. M.; Beloin, C. Biofilm-related infections: bridging the gap between clinical management and fundamental aspects of recalcitrance toward antibiotics. *Microbiol Mol Biol Rev* **2014,** *78* (3), 510-43, DOI: 10.1128/MMBR.00013-14.
(9) de la Fuente-Nunez, C.; Reffuveille, F.; Fernandez, L.; Hancock, R. E. Bacterial biofilm development as a multicellular adaptation: antibiotic resistance and new therapeutic strategies. *Curr Opin Microbiol* **2013,** *16* (5), 580-9, DOI: 10.1016/j.mib.2013.06.013.
(10) Funao, H.; Nagai, S.; Sasaki, A.; Hoshikawa, T.; Tsuji, T.; Okada, Y.; Koyasu, S.; Toyama, Y.; Nakamura, M.; Aizawa, M.; Matsumoto, M.; Ishii, K. A novel hydroxyapatite film coated with ionic silver via inositol hexaphosphate chelation prevents implant-associated infection. *Sci Rep* **2016,** *6*, 23238, DOI: 10.1038/srep23238.
(11) GhavamiNejad, A.; Park, C. H.; Kim, C. S. In Situ Synthesis of Antimicrobial Silver Nanoparticles within Antifouling Zwitterionic Hydrogels by Catecholic Redox Chemistry for Wound Healing Application. *Biomacromolecules* **2016,** *17* (3), 1213-23, DOI: 10.1021/acs.biomac.6b00039.
(12) Wu, K.; Yang, Y.; Zhang, Y.; Deng, J.; Lin, C. Antimicrobial activity and cytocompatibility of silver nanoparticles coated catheters via a biomimetic surface functionalization strategy. *Int J Nanomedicine* **2015,** *10*, 7241-52, DOI: 10.2147/IJN.S92307.
(13) Augustine, R.; Kalarikkal, N.; Thomas, S. Electrospun PCL membranes incorporated with biosynthesized silver nanoparticles as antibacterial wound dressings. *Applied Nanoscience* **2015,** *6* (3), 337-344, DOI: 10.1007/s13204-015-0439-1.
(14) Shao, W.; Wu, J.; Wang, S.; Huang, M.; Liu, X.; Zhang, R. Construction of silver sulfadiazine loaded chitosan composite sponges as potential wound dressings. *Carbohydr Polym* **2017,** *157*, 1963-1970, DOI: 10.1016/j.carbpol.2016.11.087.
(15) Wirth, S. M.; Bertuccio, A. J.; Cao, F.; Lowry, G. V.; Tilton, R. D. Inhibition of bacterial surface colonization by immobilized silver nanoparticles depends critically on the planktonic bacterial concentration. *J Colloid Interface Sci* **2016,** *467*, 17-27, DOI: 10.1016/j.jcis.2015.12.049.
(16) Percival, S. L.; Slone, W.; Linton, S.; Okel, T.; Corum, L.; Thomas, J. G. Use of flow cytometry to compare the antimicrobial efficacy of silver-containing wound dressings against planktonic Staphylococcus aureus and Pseudomonas aeruginosa. *Wound Repair Regen* **2011,** *19* (3), 436-41, DOI: 10.1111/j.1524-475X.2011.00685.x.
(17) Percival, S. L.; McCarty, S. M. Silver and Alginates: Role in Wound Healing and Biofilm Control. *Adv Wound Care (New Rochelle)* **2015,** *4* (7), 407-414, DOI: 10.1089/wound.2014.0541.
(18) Chen, Z.; Ji, H.; Liu, C.; Bing, W.; Wang, Z.; Qu, X. A Multinuclear Metal Complex Based DNase-Mimetic Artificial Enzyme: Matrix Cleavage for Combating Bacterial Biofilms. *Angew Chem Int Ed Engl* **2016,** *55* (36), 10732-6, DOI: 10.1002/anie.201605296.
(19) Li, P.; Poon, Y. F.; Li, W.; Zhu, H. Y.; Yeap, S. H.; Cao, Y.; Qi, X.; Zhou, C.; Lamrani, M.; Beuerman, R. W.; Kang, E. T.; Mu, Y.; Li, C. M.; Chang, M. W.; Leong, S. S.; Chan-Park, M. B. A polycationic antimicrobial and biocompatible

hydrogel with microbe membrane suctioning ability. *Nat Mater* **2011,** *10* (2), 149-56, DOI: 10.1038/nmat2915.
(20) Zhou, C.; Wu, Y.; Thappeta, K. R. V.; Subramanian, J. T. L.; Pranantyo, D.; Kang, E. T.; Duan, H.; Kline, K.; Chan-Park, M. B. In Vivo Anti-Biofilm and Anti-Bacterial Non-Leachable Coating Thermally Polymerized on Cylindrical Catheter. *ACS Appl Mater Interfaces* **2017,** *9* (41), 36269-36280, DOI: 10.1021/acsami.7b07053.
(21) Irawan, H.; Yasa, K. P. A case report of diabetic foot ulcer underwent an autolytic debridement using hydrogel and hydrocellular foam combination. *Bali Med. J.* **2017,** *6* (3), S93-S96, DOI: 10.15562/bmj.v3i3.411.
(22) Dong, Y. L.; Liu, W. Q.; Lei, Y. L.; Wu, T. X.; Zhang, S. W.; Guo, Y. C.; Liu, Y.; Chen, D. M.; Yuan, Q.; Wang, Y. Y. Effect of gelatin sponge with colloid silver on bone healing in infected cranial defects. *Mater. Sci. Eng. C-Mater. Biol. Appl.* **2017,** *70*, 371-377, DOI: 10.1016/j.msec.2016.09.015.
(23) Soehnlein, O.; Steffens, S.; Hidalgo, A.; Weber, C. Neutrophils as protagonists and targets in chronic inflammation. *Nat Rev Immunol* **2017,** *17* (4), 248-261, DOI: 10.1038/nri.2017.10.
(24) Eming, S. A.; Martin, P.; Tomic-Canic, M. Wound repair and regeneration: Mechanisms, signaling, and translation. *Science Translational Medicine* **2014,** *6* (265).
(25) Organization, W. H. WHO publishes list of bacteria for which new antibiotics are urgently needed.
(26) Kamarun, D.; Zheng, X.; Milanesi, L.; Hunter, C. A.; Krause, S. A peptide cross-linked polyacrylamide hydrogel for the detection of human neutrophil elastase. *Electrochimica Acta* **2009,** *54* (22), 4985-4990, DOI: 10.1016/j.electacta.2009.03.067.
(27) Wu, D.; Gao, Y.; Li, W.; Zheng, X.; Chen, Y.; Wang, Q. Selective Adsorption of La3+ Using a Tough Alginate-Clay-Poly(n-isopropylacrylamide) Hydrogel with Hierarchical Pores and Reversible Re-Deswelling/Swelling Cycles. *ACS Sustainable Chemistry & Engineering* **2016,** *4* (12), 6732-6743, DOI: 10.1021/acssuschemeng.6b01691.
(28) Kazemi, F.; Mohamadnia, Z.; Kaboudin, B.; Gharibi, H.; Ahmadinejad, E.; Taran, Z. Synthesis, characterization and swelling behavior investigation of hydrogel based on AAm and AA using CdS nanorods as photocatalyst initiator under different irradiations. *Journal of Photochemistry and Photobiology A: Chemistry* **2016,** *330*, 102-109, DOI: 10.1016/j.jphotochem.2016.07.022.
(29) Cuetos, A.; Patti, A. Equivalence of Brownian dynamics and dynamic Monte Carlo simulations in multicomponent colloidal suspensions. *Phys Rev E Stat Nonlin Soft Matter Phys* **2015,** *92* (2), 022302, DOI: 10.1103/PhysRevE.92.022302.
(30) Hisatake, K.; Tanaka, S.; Aizawa, Y. Evaporation rate of water in a vessel. *Journal of Applied Physics* **1993,** *73* (11), 7395-7401, DOI: 10.1063/1.354031.
(31) Souliotis, K.; Kalemikerakis, I.; Saridi, M.; Papageorgiou, M.; Kalokerinou, A. A cost and clinical effectiveness analysis among moist wound healing dressings versus traditional methods in home care patients with pressure ulcers. *Wound Repair Regen* **2016,** *24* (3), 596-601, DOI: 10.1111/wrr.12433.
(32) Basu, P.; Kumar, U. N.; Manjubala, I. Wound healing materials – a perspective for skin tissue engineering. *Current Science* **2017,** *112* (12), 2392-2404.
(33) Hackl, F.; Kiwanuka, E.; Philip, J.; Gerner, P.; Aflaki, P.; Diaz-Siso, J. R.; Sisk, G.; Caterson, E. J.; Junker, J. P.; Eriksson, E. Moist dressing coverage supports proliferation and migration of transplanted skin micrografts in full-thickness porcine wounds. *Burns* **2014,** *40* (2), 274-80, DOI: 10.1016/j.burns.2013.06.002.
(34) Periasamy, S.; Joo, H. S.; Duong, A. C.; Bach, T. H. L.; Tan, V. Y.; Chatterjee, S. S.; Cheung, G. Y. C.; Otto, M. How Staphylococcus aureus biofilms develop their characteristic structure. *Proceedings of the National Academy of Sciences of the United States of America* **2012,** *109* (4), 1281-1286, DOI: 10.1073/pnas.1115006109.
(35) Otto, M. Phenol-soluble modulins. *Int. J. Med. Microbiol.* **2014,** *304* (2), 164-169, DOI: 10.1016/j.ijmm.2013.11.019.
(36) Tan, N. S.; Wahli, W. Studying Wound Repair in the Mouse. *Curr Protoc Mouse Biol* **2013,** *3* (3), 171-85, DOI: 10.1002/9780470942390.mo130135.

(37) Lewis, C. L.; Craig, C. C.; Senecal, A. G. Mass and density measurements of live and dead Gram-negative and Gram-positive bacterial populations. *Appl Environ Microbiol* **2014,** *80* (12), 3622-31, DOI: 10.1128/AEM.00117-14.